iScience

CellPress
OPEN ACCESS

Article

Acetylation-induced proteasomal degradation of the activated glucocorticoid receptor limits hormonal signaling

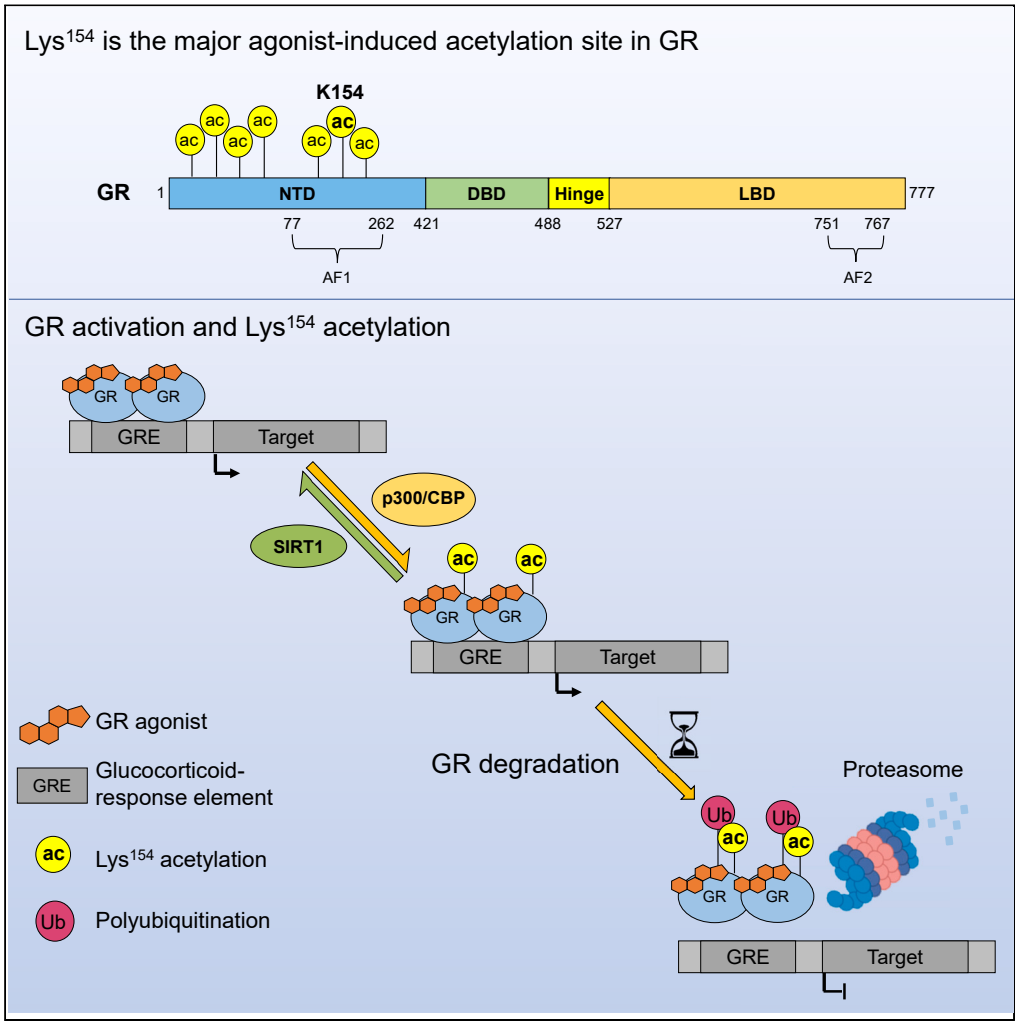

Aishwarya Iyer-Bierhoff, Martin Wieczorek, Sina Marielle Peter, ..., Karl-Heinz Guehrs, Jan P. Tuckermann, Thorsten Heinzel

t.heinzel@uni-jena.de

Highlights

Agonist-dependent GR acetylation is regulated by p300/CBP and SIRT1

Lys154 is the major acetylation site upon GR activation and nuclear translocation

Lack of acetylation increases GR stability by reducing polyubiquitination

Acetylation deficiency extends duration of GR-mediated gene regulation

Iyer-Bierhoff et al., iScience 27, 108943
February 16, 2024
https://doi.org/10.1016/j.isci.2024.108943

iScience

CellPress
OPEN ACCESS

Article

Acetylation-induced proteasomal degradation of the activated glucocorticoid receptor limits hormonal signaling

Aishwarya Iyer-Bierhoff,[1] Martin Wieczorek,[1,5] Sina Marielle Peter,[1] Dima Ward,[1] Martin Bens,[2] Sabine Vettorazzi,[3] Karl-Heinz Guehrs,[4] Jan P. Tuckermann,[3] and Thorsten Heinzel[1,6,*]

SUMMARY

Glucocorticoid (GC) signaling is essential for mounting a stress response, however, chronic stress or prolonged GC therapy downregulates the GC receptor (GR), leading to GC resistance. Regulatory mechanisms that refine this equilibrium are not well understood. Here, we identify seven lysine acetylation sites in the amino terminal domain of GR, with lysine 154 (Lys^{154}) in the AF-1 region being the dominant acetyl-acceptor. GR-Lys^{154} acetylation is mediated by p300/CBP in the nucleus in an agonist-dependent manner and correlates with transcriptional activity. Deacetylation by NAD$^+$-dependent SIRT1 facilitates dynamic regulation of this mark. Notably, agonist-binding to both wild-type GR and an acetylation-deficient mutant elicits similar short-term target gene expression. In contrast, upon extended treatment, the polyubiquitination of the acetylation-deficient GR mutant is impaired resulting in higher protein stability, increased chromatin association and prolonged transactivation. Taken together, reversible acetylation fine-tunes duration of the GC response by regulating proteasomal degradation of activated GR.

INTRODUCTION

Glucocorticoids (GCs) being lipophilic steroid hormones, traverse the cell membrane and bind to the ubiquitously expressed, cytoplasmic glucocorticoid receptor (GR) encoded by the *NR3C1* gene. Subsequently, GR translocates to the nucleus and interacts with GC-response elements (GRE) in target genes, recruiting cofactors and transcriptional modulators to activate or repress gene expression.[1–3] GC-driven transcriptional changes entail an essential pathway in stress response and restoration of homeostasis making synthetic GCs among the most commonly used anti-inflammatory therapeutics.[4] However, chronic stress, prolonged GC treatment or disease conditions such as sepsis or insulin resistance perturb functional GR levels which in turn leads to GC resistance, rendering patients unresponsive to GC-therapy.[5–8] Molecular mechanisms underlying development of GC resistance upon prolonged GC exposure are not well understood.

The human GR alpha isoform harbors an intrinsically disordered amino terminal (NTD), a central DNA binding (DBD) and a well-structured ligand binding (LBD) domain with a hinge region connecting the DBD and LBD.[9] Unlike activation function domain 2 (AF-2 or τ2) within the LBD, the AF-1 (τ1) region in the NTD is highly divergent among nuclear receptors and is implicated in gene- and cell type-specific modulation of GR transcriptional activity.[10] The AF-1 domain mediates interaction with transcriptional coregulators such as the p300 (or KAT3B)/CREB-binding protein (CBP) acetyltransferase complex.[11–14] Moreover, the NTD is subjected to phosphorylation and sumoylation that affect diverse functions such as ligand binding, localization, and gene expression.[15,16] Here we report that GR is acetylated at an NTD lysine cluster in an agonist- and transcription-dependent manner. We have identified the NAD$^+$-dependent lysine deacetylase SIRT1 and the acetyltransferase complex p300/CBP, both previously shown to interact with GR,[17,18] to be the major enzymes regulating the newly identified NTD acetylation. While GR has been reported to be acetylated at the nuclear receptor hinge region consensus motif KXKK by circadian rhythm-driving factor CLOCK,[19,20] occurrence and function of GR NTD acetylation has not been reported so far.

We found that mutation of Lys^{154} in the AF-1 is sufficient to abolish total acetylation of the receptor. In accord with downregulation of GR via the ubiquitin-proteasome pathway (UPP) regulating GR levels,[21,22] we show that acetylated GR represents an activated form of the receptor and is targeted for degradation by the UPP. This study unravels the crosstalk between acetylation and polyubiquitination of GR, linking activation-dependent modification to protein instability. We show that, over time, hyperacetylated GR undergoes targeted proteasomal

[1]Institute of Biochemistry and Biophysics, Centre for Molecular Biomedicine (CMB), Friedrich Schiller University, Hans-Knoell-Strasse 2, 07745 Jena, Germany
[2]Core Facility Next Generation Sequencing, Leibniz Institute on Aging – Fritz Lipmann Institute (FLI), Beutenbergstrasse 11, 07745 Jena, Germany
[3]Institute of Comparative Molecular Endocrinology (CME), Ulm University, Helmholtzstrasse 8/1, 89081 Ulm, Germany
[4]Core Facility Proteomics, Leibniz Institute on Aging – Fritz Lipmann Institute (FLI), Beutenbergstrasse 11, 07745 Jena, Germany
[5]Present address: IDT Biologika GmbH Dessau-Rosslau, Am Pharmapark, 06861 Dessau-Rosslau, Germany
[6]Lead contact
*Correspondence: t.heinzel@uni-jena.de
https://doi.org/10.1016/j.isci.2024.108943

degradation more robustly than an acetylation-deficient mutant, curbing the GC cascade. Conversely, SIRT1 mediated deacetylation extends GR half-life, sustaining hormone responsiveness at prolonged treatment times.

RESULTS

GR acetylation is regulated by p300/CBP and SIRT1 in a dexamethasone-dependent manner

Using mutational analysis within a lysine cluster in the hinge region, previous reports have shown GR to be acetylated.[19,20] However, a systematic analysis of GR acetylation and identification of the modifying enzymes remains open. To fill this gap, we first monitored synthetic GC, dexamethasone (Dex)-dependent GR acetylation in different cell lines by immunoprecipitation of ectopic FLAG-tagged GR and immunoblotting with anti-pan acetyl-lysine antibody. GR acetylation was detectable only in Dex- and not in vehicle (veh)- treated cells, implicating the requirement of a ligand for this modification (Figure 1A). Hereafter the term 'GR acetylation' refers to 'Dex-dependent GR acetylation'. To identify the lysine acetyltransferase (KAT), we individually overexpressed the major nuclear KATs (CBP, p300, PCAF, GCN5 and TIP60) together with FLAG-GR, followed by immunoprecipitation of GR and western blot analysis of acetylation. Only the overexpression of p300, and to a lesser extent CBP, boosted acetylation of GR indicating p300/CBP to be the prime GR acetylating enzymes (Figures 1B and S1A). This finding was confirmed by siRNA- and shRNA-mediated knockdown of p300 and CBP decreasing Dex-induced acetylation of GR, respectively (Figure S1B). To identify the histone deacetylase(s) (HDACs) responsible for removal of the acetyl group, we scrutinized acetylation in cells treated with Dex in combination with HDAC inhibitors (HDACi) such as trichostatin A (TSA) a class I, II and IV HDACi, nicotinamide (NAM) a class III HDACi (pan sirtuin inhibitor), or the selective SIRT1 inhibitor, Ex527. Inhibition of sirtuins and particularly that of SIRT1 led to an elevated GR acetylation (Figures 1C and S1C). Class I HDACs such as HDAC1/2/3 have been postulated to target GR acetylation.[19,23] To investigate this, we monitored Dex-driven GR acetylation in cells treated with siRNAs against HDACs 1, 2, 3 or SIRT1. While knockdown of all tested deacetylases was highly efficient, only the depletion of SIRT1 showed an increasing GR acetylation tendency, corroborating that SIRT1 is the predominant deacetylase of GR (Figures 1D and S1D). Conversely, overexpression of the wild-type but not the catalytically inactive mutant (H363Y) SIRT1 attenuated GR acetylation indicating that SIRT1 deacetylase activity is required to lower GR acetylation (Figure S1E). To demonstrate that GR is a direct target of SIRT1, we performed an *in vitro* deacetylation assay. To this end, hyperacetylated GR immunoprecipitated from cells treated with Dex and Ex527 was incubated with purified recombinant human SIRT1 (rhSIRT1) in the presence or absence of its cofactor NAD^+ in combination with or without SIRT1i, Ex527. While GR was deacetylated in the presence of both 1 and 3 units of SIRT1, Ex527 treatment inhibited this *in vitro* deacetylation activity albeit to different extents depending on the amount and batch of rhSIRT1 used (Figures 1E and S1F). Nevertheless, GR was efficiently deacetylated in an NAD^+- and SIRT1-dependent manner proving that GR is a direct substrate of SIRT1 (Figures 1E and S1F).

Lys^{154} is the major Dex-induced acetylation site

To assess the SIRT1-targeted acetylation sites in GR, mass spectrometric analyses were performed. LC-MS/MS analyses of immunoprecipitated FLAG-GR from cells treated with Dex in combination with Ex527 or NAM revealed acetylation at lysine residues (K) 31, 40, 57, 67, 140, 154 and 171, the latter three being within the regulatory AF-1 (τ1) region (Figures S2A–S2H). To identify the dominant acetyl acceptor site, we generated acetylation-deficient mutants of GR where lysine was substituted with arginine (K→R). Immunoprecipitation followed by western blotting with the pan acetyl-lysine antibody showed that while wild-type (WT) GR was acetylated upon Dex treatment, mutating all seven lysines (7KR) or only the three lysines within the AF-1 domain (τ1-KR) abolished GR acetylation (Figure 2A- see lanes 1, 5, 6). Single point mutation of Lys^{154}, but not of Lys^{140} or Lys^{171} within the AF-1 domain, was sufficient to phenocopy τ1-KR or 7KR indicating that Lys^{154} is the major Dex-induced acetylation site (Figure 2A lanes 1, 2, 3, 4). Multiple sequence alignment revealed that Lys^{154} is well conserved among mammalian GR (Figure 2B). We generated site-specific antibodies against acetyl-Lys^{154} (anti-acK154) to enable immunodetection in whole cell extracts. To validate the specificity of the antibody, we engineered HEK293 cells (fast-growing and highly amenable to transfections) using CRISPR/Cas9 to knockout the endogenous GR (HEK293 $GR^{-/-}$) (Figure S4B shows knockout efficiency) and transiently expressed wild-type (WT) or acetylation-deficient or -mimetic mutants, K154R or K154Q respectively. Immunoprecipitation with anti-FLAG antibodies followed by western blotting with a pan acetyl-lysine antibody displayed Dex-dependent acetylation signal of the WT but not of the mutant GR, confirming Lys^{154} is the major acetylated residue (Figure 2C- upper panel). Notably, the acetylation-mimetic K154Q mutant was unable to restore total acetylation indicating the lack of a true acetylation-mimicking phenotype of GR (Figure 2C- upper panel). Immunoblot analysis of whole cell lysates with anti-acK154 antibody detected acetylated WT- but not K154R- or K154Q-GR in Dex-treated conditions, verifying the specificity of the site-specific acetylation antibody (Figure 2C- lower panel). GR being a ubiquitously expressed nuclear receptor, we investigated whether the acK154 modification is induced in different cell types in response to Dex. Indeed, western blotting with anti-acK154 antibody showed GR acetylation in human and mouse cell lines treated *in vitro*, primary human umbilical vein endothelial cells (HUVEC) treated *ex vivo* or in tissue lysates from mice treated *in vivo*, with Dex (Figures 2D and 2E) presenting this mark to be a cell-type independent, ubiquitous modification. In line with SIRT1 and p300/CBP being the main enzymes modulating GR acetylation, their inhibition with the small molecules Ex527 and A485 led to increased and decreased levels of acK154 respectively (Figures 2F and 2G). Moreover, knockdown or overexpression of SIRT1 but not of another nuclear sirtuin, SIRT7, resulted in a concomitant increase or reduction in Dex-induced acK154 levels respectively, underscoring acK154 to be regulated by SIRT1 (Figures S2I and S2J).

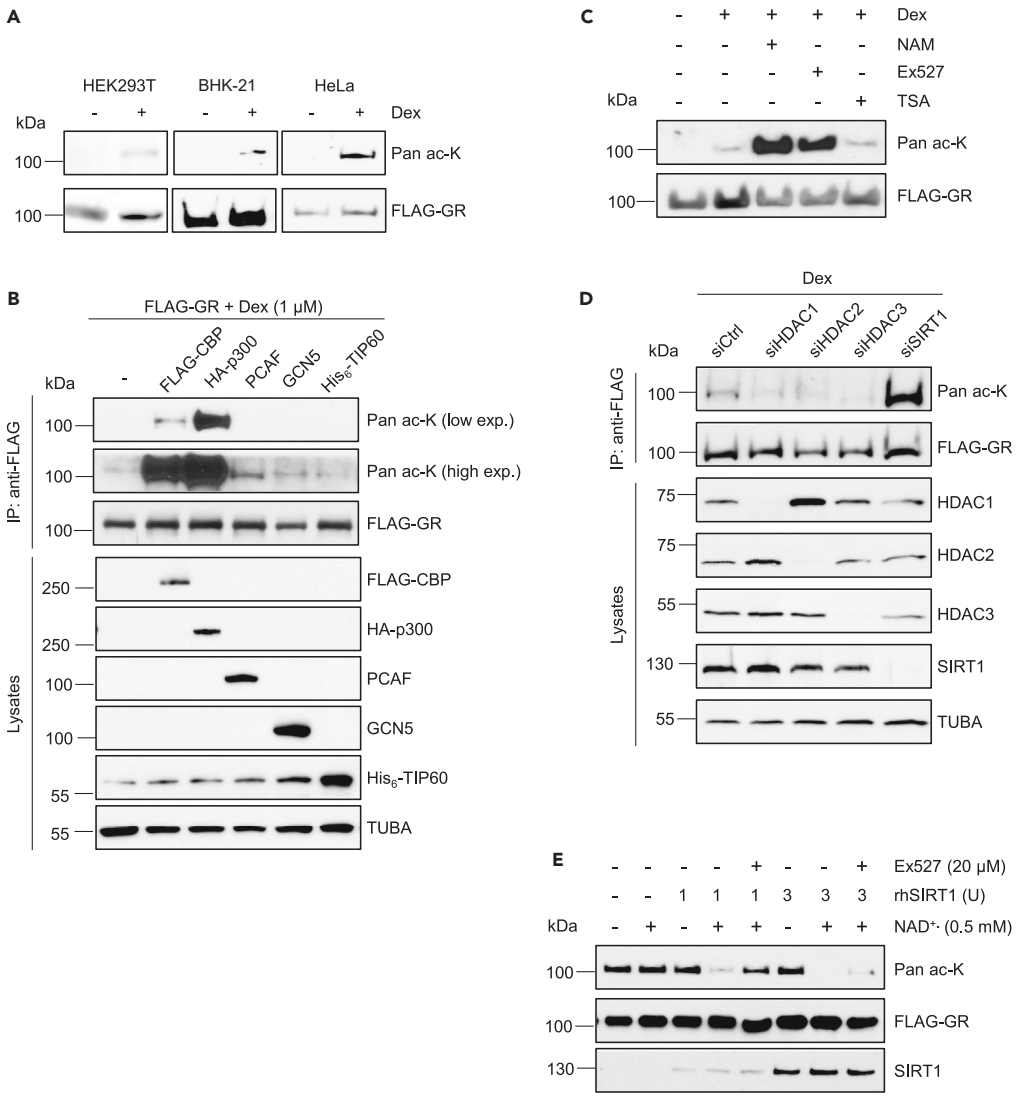

Figure 1. GR acetylation is regulated by p300/CBP and SIRT1 in a dexamethasone-dependent manner

Western blot analyses with pan acetyl-lysine (ac-K) and FLAG antibodies, showing acetylation levels of immunoprecipitated FLAG-GR under the following experimental conditions.

(A) The indicated cell lines were treated with 1 μM Dex or vehicle for 6 h.

(B) HeLa cells transiently overexpressed the individual lysine acetyltransferases (KATs) and were treated with 1 μM Dex for 16 h. Immunoblot of whole cell lysates indicates expression levels of the overexpressed KATs.

(C) HeLa cells treated with vehicle or 1 μM Dex in combination with the pan sirtuin inhibitor NAM (10 mM) or the selective SIRT1 inhibitor Ex527 (20 μM) or the class I and II HDACi TSA (1 μM) for 6 h.

(D) HeLa cells were transfected with siRNAs against the indicated histone deacetylases followed by treatment with vehicle or 1 μM Dex for 16 h. Western blotting of whole cell lysates show knockdown efficiency of the individual HDACs.

(E) *In vitro* deacetylation assay. Immunopurified, hyperacetylated FLAG-GR from BHK-21 cells, was incubated with 1 or 3 units (U) of recombinant human (rh)SIRT1 in the presence or absence of NAD^+ and Ex527 as indicated.

See also Figure S1.

Lys^{154} acetylation is agonist-dependent and is associated with ongoing transcription

To determine if acK154 is induced in a ligand-dependent manner, liver-derived HepG2 and lung-derived A549 cells were treated with vehicle or equimolar concentrations of three different synthetic GCs Dex, prednisolone (Pred) or hydrocortisone (Hydro) respectively. These GCs display variable potency, kinetics and bioavailability depending on the target cell type.[24,25] As expected, agonist treatment elevated the expression of a bona fide GR target gene, GC-induced leucine zipper, *GILZ* (or *TSC22D3*) albeit to different extents depending on the GC potency and the cell type (Figures 3A and S3A) (HepG2: Dex = Pred > Hydro; A549: Dex = Pred = Hydro). Concomitantly, the acK154

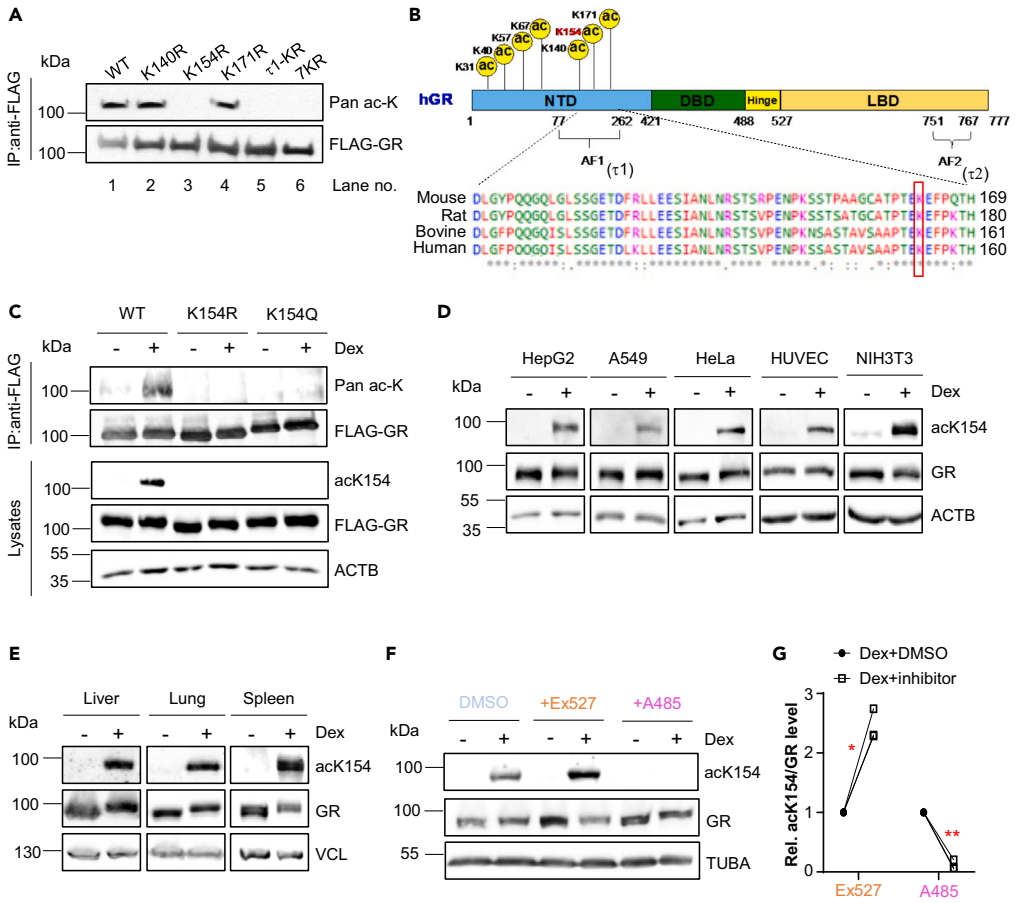

Figure 2. Lys^{154} is the major Dex-induced acetylation site

(A) Western blot analysis with pan acetyl-lysine (ac-K) detecting acetylation levels of the FLAG-tagged GR-wild-type (WT) or Lys to Arg mutants of the individual AF-1 acetylation sites, all three (τ1-KR), and all seven residues in the NTD (7KR), immunoprecipitated from BHK-21 cells that were treated with vehicle or 1 μM Dex for 6 h.

(B) Scheme indicating position of the acetylated lysines in the N-terminal domain of hGR. Lys^{154} is marked in red and its conservation among murine, rat, bovine and human GR is shown in the multiple sequence alignment below. Color scheme indicating amino acid properties and consensus symbols is as outlined by CLUSTAL Omega.

(C) Western blot detection of global GR acetylation with pan acetyl-lysine antibody or GR-K154 acetylation with the site-specific anti-acK154 antibodies in FLAG immunoprecipitates (top:IP) and whole cell lysates (bottom) prepared from HEK293 GR$^{-/-}$ cells transiently expressing wild-type or mutant FLAG-GR and treated with vehicle or 1 μM Dex for 6 h.

(D) Western blot monitoring endogenous GR-K154 acetylation in lysates from vehicle or Dex (1 μM, 6 h) treated human (HepG2, A549 and HeLa), primary human umbilical vein endothelial cells (HUVEC) and mouse fibroblast (NIH3T3) cell lines. Beta actin (ACTB) served as loading control.

(E) Western blot analysis of GR-K154 acetylation in tissue lysates derived from liver, lung and spleen of C57BL/6 mice treated with vehicle or 1 mg/kg Dex (i.p) for 6 h. Vinculin (VCL) served as loading control.

(F) Immunoblot of GR-K154 acetylation in vehicle- or Dex- (1 μM, 6 h) treated HepG2 cells that were co-treated with DMSO (as control), 20 μM Ex527 or 5 μM A485 respectively.

(G) Ratios of acK154 to GR western blot signals from (F) were quantified and normalized to Dex+DMSO sample and represented as relative acK154/GR (Mean ± S.E.M; n = 3 independent experiments, *p < 0.05, **p < 0.01; Welch's t-test).

See also Figure S2.

level induced by the three agonists in both cell types was correlated with induction of *GILZ* expression levels, linking acK154 to GR-mediated transactivation potential (Figures 3B and S3B). Ligand binding triggers conformational changes and nuclear translocation of GR, bringing it in proximity of the nuclear acetyltransferase p300/CBP. To investigate whether acK154 is merely a coincidence of nuclear translocation or if it has a functional role, we monitored GR acK154 in cells treated with the agonist Dex or the GR antagonist RU486 (mifepristone) and subjected to fractionation to yield cytoplasmic and nuclear extracts. As expected, treatment with Dex and RU486 prompted nuclear localization of GR albeit to a lesser extent by the antagonist (Figure 3C). However, acK154 was detectable only in the nuclear fraction of Dex-treated cells highlighting that acK154 is induced in an agonist-dependent manner (Figure 3C). Co-treatment of RU486 with Dex impaired Dex-driven

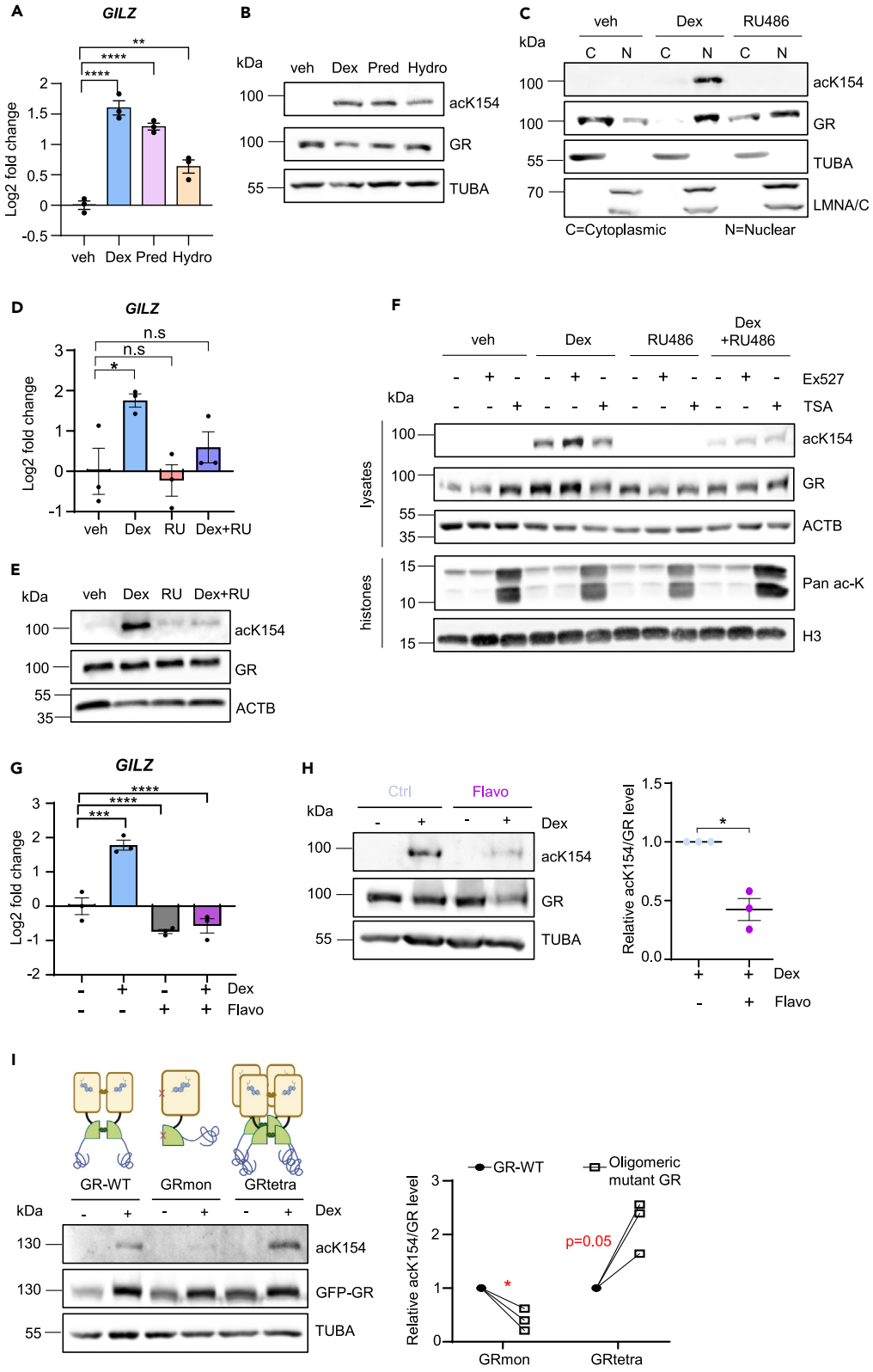
A
GILZ
Log2 fold change
veh Dex Pred Hydro
B
kDa
veh Dex Pred Hydro
acK154
GR
TUBA
C
veh Dex RU486
C N C N C N
acK154
GR
TUBA
LMNA/C
C=Cytoplasmic
N=Nuclear
D
GILZ
n.s
Log2 fold change
veh Dex RU Dex+RU
E
veh Dex RU Dex+RU
acK154
GR
ACTB
F
veh Dex RU486 Dex +RU486
Ex527
TSA
lysates
histones
acK154
GR
ACTB
Pan ac-K
H3
G
GILZ
Log2 fold change
Dex
Flavo
H
Ctrl
Flavo
Dex
acK154
GR
TUBA
Relative acK154/GR level
I
GR-WT
GRmon
GRtetra
Dex
acK154
GFP-GR
TUBA
Oligomeric mutant GR
p=0.05
Relative acK154/GR level

Figure 3. Lys^{154} acetylation is agonist-dependent and correlates with GR activation

(A) RT-qPCR analysis of *GILZ* expression levels in HepG2 cells treated with vehicle or 1 μM each of Dex or prednisolone (Pred) or hydrocortisone (Hydro) respectively for 6 h.

(B) Western blot detection of GR-K154 acetylation in cells treated as in (A).

(C) Subcellular fractionation showing distribution of GR-K154 acetylation, GR and bona fide cytoplasmic (C) and nuclear (N) markers alpha-tubulin (TUBA) and lamin A/C (LMNA/C) respectively in fractions of HepG2 cells that were treated with vehicle or 1 μM each of Dex or RU486 for 6 h.

(D) RT-qPCR analysis of *GILZ* expression levels in HepG2 cells treated with vehicle or 1 μM each of Dex, RU486 or both, for 6 h.

(E) Western blot image of GR-K154 acetylation in whole cell lysates from HepG2 cells treated as in (D).

(F) Western blot analysis of GR-K154 acetylation in whole cell lysates (top panel) or histone acetylation with pan-acetyl lysine antibody in histone preparations (bottom panel). HepG2 cells were treated with vehicle or 1 μM each of Dex or RU486 with 20 μM Ex527 or 1 μM TSA, respectively for 6 h. TUBA and histone H3 serve as respective loading controls.

(G) RT-qPCR of *GILZ* mRNA in cells treated with Pol II inhibitor, flavopiridol (1 μM) in combination with vehicle or 1 μM Dex for 6 h.

(H) Western blot monitoring the effect of transcription inhibition on GR-K154 acetylation in HepG2 cells treated as in (G). Quantification is shown in the graph on the right.

(I) Western blot image showing GR-K154 acetylation of GFP-tagged mGR wild-type (WT) or monomeric (mon) or tetrameric (tetra) mutants (indicated in the scheme in the top panel) transiently expressed in HEK293 GR$^{-/-}$ cells treated with vehicle or 1 μM Dex for 6 h. Quantification is shown in the graph on the right. Data in (H) and (I) represent ratios of acK154 to GR western blot signals normalized to the Dex alone (H) or to the WT-Dex (I) sample and represented as relative acK154/GR in the graphs on the right. n = 3 independent experiments; Welch's t-test, *p < 0.05, n.s: non-significant. Data in (A), (D) and (G) represent mean of log2 fold change values from n = 3 independent experiments. Error bars = S.E.M. *p < 0.05, **p < 0.01, ***p < 0.001, n.s = non-significant; One-way ANOVA-Fischer's LSD test.

See also Figure S3.

GILZ expression as well as Dex-induced acK154 (Figures 3D and 3E). Moreover, titration of RU486 along with a single dose of Dex hindered GR acK154 in two different cell lines in a dose-dependent manner, suggesting a universal mechanism underlying the antagonistic effect of RU486 on acK154 (Figures S3C–S3E). In accordance with Lys^{154} being the major acetylation site, RU486 attenuated not only acK154 but also global acetylation of GR as detected by immunoprecipitation and pan acetyl-lysine immunoblots (Figure S3F). Agonists and antagonists have been shown to differentially alter GR conformation, thereby recruiting transcriptional coactivators or corepressors respectively.[26] To determine whether RU486-mediated attenuation of acK154 is due to engagement of a deacetylase, cells were treated with Dex or RU486 in combination with the SIRT1i Ex527 and the pan HDACi TSA respectively. While Ex527 and TSA accentuated GR-acK154 and histone acetylation respectively, RU486-dependent reduction of the acK154 signal was not reversed by either of the inhibitors, indicating that RU486 most likely hinders the induction of acetylation rather than promoting the deacetylation of GR (Figure 3F). To elucidate whether GR acK154 is dependent on ongoing transcription, we treated cells with the RNA polymerase II inhibitor, flavopiridol in addition to Dex. Flavopiridol treatment profoundly suppressed transcript levels of *GILZ* along with a decrease in the Dex-induced GR K154 acetylation signal, emphasizing that acK154 is a co-transcriptional modification of GR (Figures 3G and 3H). Mutation of residues in the DBD and LBD have been shown to interfere with the oligomerization interface of GR and thereby impact GR activity, the tetrameric form being most active and the monomer having lowest transcriptional activity.[27,28] Immunodetection of acK154 levels of wild-type and the oligomeric point mutants of murine GR transiently expressed in the easy-to-transfect HEK293 GR$^{-/-}$ cells, revealed that acetylation status correlated with the oligomeric state, the constitutively tetrameric mutant (P481R) showing increased acetylation, while the monomeric (A465T/I634A) form showing minimal acetylation (Figure 3I). Taken together, these results highlight agonist-dependent acK154 to be an activation mark of GR associated with GR transcriptional activity.

Acetylation-deficient GR sustains transcription longer than the wild-type

Having shown that GR-acK154 is a universal mark induced in several cell lines and mouse tissues in an agonist-dependent manner, we focused our further functional analyses in hepatocyte-derived HepG2 cells owing to well-known functions of GR in the liver.[29] To evaluate the direct impact of GR acK154 on target gene expression, stable cell lines expressing acetylation-deficient and -mimetic mutants of GR were generated by Lys^{154} to Arg (K→R) or Lys^{154} to Gln (K→Q) substitutions respectively. Firstly, CRISPR/Cas9 mediated gene engineering was used to knockout the endogenous GR (Gene: *NR3C1*) in HepG2 cells (HepG2 GR$^{-/-}$). Three sgRNAs targeting exon 2 regions corresponding to the NTD of GR were used (Figure S4A; Table S3) and western blot analysis revealed complete deletion of GR with no remaining GR truncation forms or isoforms (Figure S4B). Moreover, the GR knockout cells failed to activate a luciferase reporter driven by the GC-responsive mouse mammary tumor virus (MMTV) promoter[30] (Figure S4C) confirming the loss of functional GR. The HepG2 GR$^{-/-}$ cells were further transduced with lentiviral constructs to individually express Ty1-tagged WT-, K154R- or K154Q-GR in a doxycycline (Dox)-inducible manner (Figure S4D). Expression levels of the reconstituted Ty1-GR variants were matched to endogenous GR levels in wild-type HepG2 cells and to each other by titrating Dox dosage (see STAR Methods for details) (Figure 4A). K154R- and K154Q-GR mutants showed Dex-dependent nuclear import like WT-GR (Figure S4E) corroborating that transgenic GR forms are functional in the cell lines created. Notably, WT and both K154 mutants of GR increased MMTV-driven luciferase activity after Dex treatment for 6 h as compared to vehicle-treated cells, suggesting that acK154 does not impact GR-mediated transactivation under these conditions (Figure 4B). To investigate whether GR acK154 has a gene-specific transcriptional effect, we performed RNA sequencing analysis of GR$^{-/-}$ + WT, GR$^{-/-}$ + K154R and GR$^{-/-}$ + K154Q cells that were treated with vehicle or 1 μM Dex for 6 h. Each genotype showed Dex-dependent gene expression changes (mostly upregulation) as compared to vehicle-treated controls, which were termed as differentially expressed genes (DEGs) for each cell line or genotype using

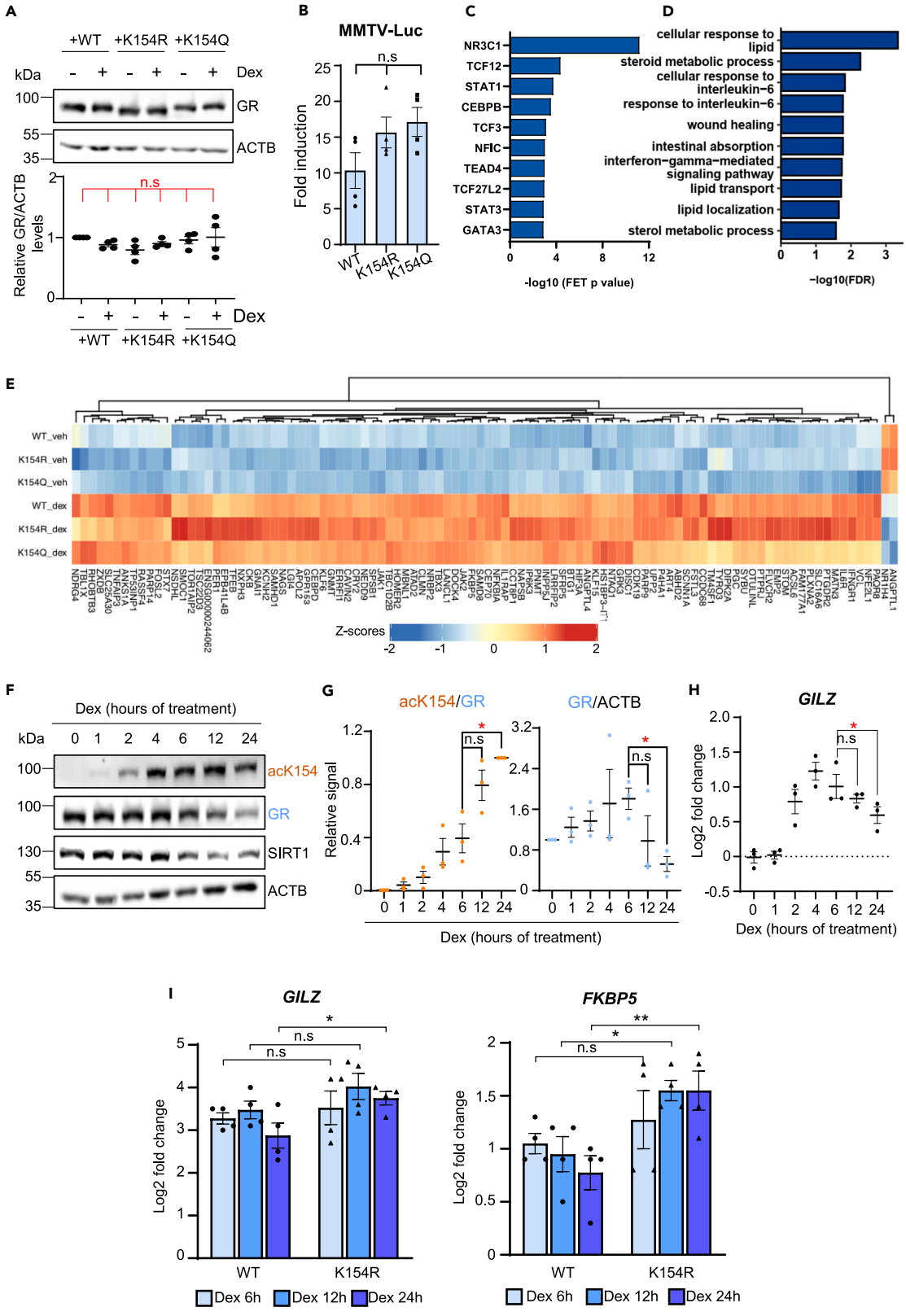
A
+WT +K154R +K154Q
kDa - + - + - + Dex
100
GR
55
ACTB
35
Relative GR/ACTB levels
n.s
- + - + - + Dex
+WT +K154R +K154Q
B
MMTV-Luc
n.s
Fold induction
WT
K154R
K154Q
C
NR3C1
TCF12
STAT1
CEBPB
TCF3
NFIC
TEAD4
TCF27L2
STAT3
GATA3
-log10 (FET p value)
D
cellular response to lipid
steroid metabolic process
cellular response to interleukin−6
response to interleukin−6
wound healing
intestinal absorption
interferon−gamma−mediated signaling pathway
lipid transport
lipid localization
sterol metabolic process
−log10(FDR)
E
WT_veh
K154R_veh
K154Q_veh
WT_dex
K154R_dex
K154Q_dex
Z-scores
-2 -1 0 1 2
F
Dex (hours of treatment)
kDa 0 1 2 4 6 12 24
100
acK154
100
GR
130
SIRT1
55
ACTB
35
G
acK154/GR
GR/ACTB
Relative signal
n.s
Dex (hours of treatment)
H
GILZ
Log2 fold change
n.s
Dex (hours of treatment)
I
GILZ
FKBP5
Log2 fold change
n.s
WT
K154R
Dex 6h
Dex 12h
Dex 24h

Figure 4. Acetylation-deficient GR sustains transcription longer than the wild-type

(A) Western blot showing doxycycline-induced expression of wild-type and mutant GR in stably transduced HepG2 $GR^{-/-}$ cells treated with vehicle or 1 μM Dex for 6 h. Quantification below shows relative GR/ACTB levels normalized to WT veh sample from n = 4 independent experiments. n.s = non-significant; Welch's ANOVA with Dunnett's T3 post hoc test.

(B) Luciferase assay detecting MMTV-driven luciferase expression in cells treated as in (A) expressed as fold induction to respective vehicle controls.

(C) ChEA3 analysis of the 100 commonly regulated DEGs showing top 10 enriched transcription factors (TFs). Y axis shows names of TFs and X axis indicates negative logarithm of Fischer's exact test (FET) p-values.[31]

(D) Gene ontology analysis indicating biological processes enriched among the common DEGs.

(E) Heatmap showing expression of all Dex-regulated genes common between WT-, K154R- and K154Q-GR mutants as identified by RNA-seq analysis.

(F) Western blot showing GR-K154 acetylation, GR and SIRT1 levels in HepG2 cells over a time course of 1 μM Dex treatment (0–24 h). ACTB serves as loading control.

(G) Ratios of acK154 to GR (orange) or GR to ACTB (blue) western blot signals from (F) were quantified and normalized to 24 h Dex sample or vehicle (0 h Dex) sample respectively and represented as relative signal.

(H) RT-qPCR showing expression of *GILZ* as log2 fold change in cells treated as in (F).

(I) RT-qPCR showing expression of *GILZ* as log2 fold change to vehicle after 6 h, 12 h and 24 h Dex treatments in HepG2 $GR^{-/-}$ + WT-GR or HepG2 $GR^{-/-}$ + K154R cell lines.

Data represent mean from n = 4, except for (G, H) where n = 3, independent experiments. Error bars = S.E.M *p < 0.05, **p < 0.01, ****p < 0.0001, n.s = non-significant; One way ANOVA- Fischer's LSD test (G, H, I).

See also Figure S4, Tables S1 and S2.

FDR<0.05 threshold (Table S1). Principal component analysis revealed that the DEGs grouped into vehicle- and Dex-treated sets without a clear separation between the genotypes (WT- or mutant- GR), indicating that K154 acetylation does not fundamentally alter the repertoire of GR target genes (Figure S4F). The majority (100) of DEGs were commonly regulated and formed ~58%, ~55% and ~72% of all DEGs from WT-, K154R- and K154Q-GR cells respectively (Figure S4G; Table S1). As each of the genotypes showed 'unique' DEGs (45 in WT, 55 in K154R and 12 in K154Q) with FDR<0.05 (Figure S4G), we performed Likelihood ratio test (LRT) to directly test for significant differences in the magnitude or direction of log2 fold changes between the genotypes in response to Dex-treatment. LRT revealed no genes that show a robust difference in their response to Dex when comparing between genotypes, indicating that the 'unique' DEGs do not significantly differ between WT and mutants with respect to their log2 fold change (Table S2). Therefore, we performed transcription factor enrichment analysis of the 100 common DEGs using ChEA3[31] which ranked GR (NR3C1) to be the predominant regulatory factor associated with the gene set rendering this dataset to be of high confidence (Figure 4C). Moreover, gene ontology analysis of the common DEGs revealed enrichment of the biological process terms related to lipid and steroid metabolism (Figure 4D) in line with the reported transcriptional program driven by hepatic GR.[29,32] Closer inspection of the magnitude of gene expression changes disclosed that all three GR variants affected the common DEGs to a similar extent with K154R and K154Q showing an overall more robust or a milder impact than WT, respectively (Figure 4E). However, LRT did not reveal these differences to be significant (Table S2), indicating that WT and mutant GR show similar Dex-dependent target gene modulation at 6 h of treatment.

The stoichiometry of a post-translational modification is important in determining its biological relevance and impact on protein function.[33] To estimate the relative stoichiometry of GR-K154 acetylation, we performed sequential immunoprecipitation (Seq-IP) of total GR followed by pulldown with the anti-acK154 antibody (Figure S4H, scheme). For this, we expressed FLAG-GR in HEK293 $GR^{-/-}$ cells, treated with vehicle or 1 μM Dex for 6 h followed by lysis and seq-IP. Immunoprecipitation with anti-FLAG M2 beads depleted the flow-through (F.T1) (Figure S4H, lanes 5, 6; GR panel) and enriched the eluate1 (Figure S4H, lanes 9, 10; GR panel) with the entire FLAG-GR population in vehicle- and Dex-treated cells whereas control IP with IgG did not (Figure S4H, lanes 3,4 and 7,8). Subsequent anti-acK154 IP using eluate1 IgG and eluate1 M2 as inputs (input2) was performed. While acK154 IP from the IgG eluates (IgG input2) revealed no specific IP and only background (Figure S4H, lanes 19, 20-acK154 panel), acK154 IP from M2 input2 completely depleted acetylated GR (Figure S4H, lane 18; acK154 panel) and enriched acetylated GR in eluates from the Dex sample underscoring a high efficiency of acK154 IP (Figure S4H, lane 22; acK154 panel). Flow-through fraction from the acK154 IP (F.T2) showed a similar signal for FLAG-GR in vehicle- and Dex-treated samples (Figure S4H, lanes 17, 18; GR panel). Anti-acK154 IP depleted all acK154-GR but only a negligible amount of FLAG-GR from F.T2 (Figure S4H, lanes 18, 22; acK154 and GR panels) indicating that only a minor fraction of GR is acetylated at 6 h of Dex treatment rendering the majority of GR to be deacetylated.

Thus, to understand the functional role of GR K154 acetylation, we followed the Dex-dependent acK154 level changes over time. In line with downregulation of GR with prolonged GC treatment,[34] GR protein level rose slightly in the first 6 h followed by a steady and significant drop (Figures 4F and 4G). Contrarily, the relative acK154 to GR levels increased with treatment duration and plateaued between 12 and 24 h when GR levels were at their lowest (Figures 4F and 4G). Moreover, the level of the GR deacetylase, SIRT1 was reduced in the course of Dex treatment, likely contributing to a concomitant increase in acK154 (Figure 4F). Measurement of *GILZ* expression levels also showed a trend akin to GR levels (Figure 4H), raising the question if GR reduction, or the relative increase in acK154 level impacted gene activity upon prolonged Dex exposure. To test these possibilities, we aimed to compare transcriptional activity of hyperacetylated and non-acetylated GR. As the K154Q mutant failed to faithfully mimic acetylated GR (Figure 2C- upper panel)[35] and showed no striking differences to the K154R mutant, we monitored GR target gene expression by RT-qPCR after 6, 12 and 24 h of Dex treatment in $GR^{-/-}$ + WT and $GR^{-/-}$ + K154R cells. Dex-dependent induction of *GILZ* and *FKBP5* (FK506 binding protein 5) mRNA levels was similar after 6 h but was augmented more in $GR^{-/-}$ + K154R than $GR^{-/-}$ + WT after 12 and 24 h (Figure 4I), indicating that acetylation-deficient GR outperforms wild-type GR at prolonged Dex exposure by sustaining transcription at target genes.

GR acetylation attenuates chromatin binding and protein stability upon prolonged GC exposure

To address whether acetylation of GR impairs its localization to glucocorticoid response elements (GRE) upon prolonged Dex exposure, we performed chromatin immunoprecipitation (ChIP) of wild-type and K154R-GR after 24 h of Dex treatment. K154R-GR exhibited higher chromatin occupancy at *GILZ* and *FKBP5* GREs as compared to that of wild-type GR (Figure 5A). Subnuclear fractionation of cells expressing wild-type and mutant GR after 6 and 24 h of Dex treatment indicated that the mutant GR has higher global chromatin retention as compared to the wild-type protein (Figure S5). These results postulate that acetylated GR is removed from DNA binding sites at a faster rate than acetylation-deficient GR. To monitor the protein stability in response to Dex, we performed a chase assay with the translation inhibitor cycloheximide (CHX), comparing wild-type and K154R-GR levels up to 24 h. Pre-treatment with Dex followed by a CHX time course, revealed that wild-type GR was degraded faster than the K154R-mutant (Figure 5B). Furthermore, GR protein stability was lower in combinatorial treatment of Dex and Ex527 as compared to Dex alone, underscoring that the hyperacetylated GR form is less stable (Figure 5C). As there is a precedent for ubiquitin proteasome system-dependent removal of transcription factors from DNA binding sites,[36] we monitored polyubiquitination of immunoprecipitated GR. To this end, HEK293 $GR^{-/-}$ cells transfected with FLAG-tagged WT- or K154R-GR in combination with HA-tagged ubiquitin (UBB) were co-treated with Dex and the proteasomal inhibitor, MG132 for 24 h followed by anti-FLAG immunoprecipitation and western blotting with anti-HA antibody. Wild-type GR showed increased levels of polyubiquitination as seen by stronger relative signal for higher molecular weight bands as compared to that of K154R-GR upon Dex+MG132 treatment (Figure 5D). Taken together, these results emphasize that p300/CBP-dependent GR acetylation earmarks the activated receptor for polyubiquitination and subsequent proteasomal elimination from chromatin sites, thereby dampening the transcriptional response to GCs.

DISCUSSION

In the last two decades, acetylation of nuclear receptors has emerged as a common regulatory modification altering localization, DNA binding and transcriptional signaling in health and disease.[38] In line with the reported acetylation of lysine residues within the conserved hinge region of steroid receptors, Lys^{494} and Lys^{495} within the C-terminus of GR were shown to be regulated by HDAC2 and CLOCK/BMAL1.[19,20] While both studies employed pan acetyl-lysine antibody and site-directed mutagenesis to showcase acetylation, direct evidence by mass spectrometry (MS) was not shown. Moreover, mutation of Lys^{494} and Lys^{495} did not abolish Dex-dependent acetylation of GR[19] indicating the presence of other acetylation sites. Trypsin cleaves specifically after arginine and lysine residues except when they harbor modifications such as acetylation, that renders resistance to tryptic digestion due to steric hindrance. Moreover, in the presence of tandem, unmodified arginine or lysine residues, trypsin generates very short peptides which are not detectable by MS.[39] Owing to the presence of consecutive lysine residues in the hinge region that are most likely not acetylated under the given conditions, our MS analysis of tryptic peptides was unable to detect the reported acetyl-lysines. In the current work, we report the identification of lysine acetylation in the intrinsically disordered NTD of GR by LC-MS/MS. Mutation of Lys^{154} within the AF-1 was sufficient to abolish Dex-dependent GR acetylation rendering it the major site of modification (Figure 2A) and possibly serving as an initiator site for acetylation at other lysine residues across the GR peptide sequence. We therefore generated a site-specific acK154 antibody as a proxy for GR acetylation which was detectable across several human cell lines and mouse tissues (mGR: Lys^{163}) upon *in vitro* or *in vivo* GC treatment, underscoring the cell-type independent occurrence and the physiological relevance of this modification.

In line with agonist binding to the LBD inducing a conformational change conducive to coactivator recruitment to the AF-1 region,[10,40] p300/CBP was found to be the major acetyltransferase of GR in the presence of the synthetic GC Dex. Quantitative acetylomics revealed that p300/CBP modifies several enhancer-associated transcription regulators.[41] Based on the finding that GR interacts with p300 at chromatin sites,[16] it is conceivable that agonist-bound GR undergoes nuclear translocation and binds to coactivators such as p300/CBP at gene regulatory elements and is subsequently modified in a co-transcriptional manner (Figure 3). Acetylation of GR at regulatory elements bound by p300 may create a local transcription factor activity gradient regulating promoter activation and gene transcription.[42] Clustered acetylation of multiple lysine residues in GR may function as a high affinity platform for the recruitment of bromodomain-containing proteins and subsequent activation of transcription.[43] Moreover, p300 sequestration at GR binding sites in activated and repressed gene loci suggests that p300-dependent GR acetylation may not only be associated with transactivation but also with transrepression.[44] Although antagonists such as RU486 drive nuclear translocation of GR, the recruitment of corepressors, such as histone deacetylases, instead of coactivators such as p300/CBP, results in antagonist activity.[45] Co-treatment with deacetylase inhibitors did not rescue RU486-dependent repression of acK154 indicating an interference in the interaction between antagonist-bound GR and p300/CBP (Figure 3F). Similarly, RU486 does not induce phosphorylation at Ser^{211},[46] underscoring that acK154 serves as a marker for GR activation status. Reminiscent of Ser^{211} phosphorylation altering AF-1 conformation to recruit coactivators,[40] acK154 might bolster this effect. As the GR AF-1 is subjected to several phosphorylations in response to ligand binding,[15] further investigation of the crosstalk between acetylation and phosphorylation might provide insights into co-regulatory functions.

SIRT1, which has been reported to be an enhancer of GR activity,[18] was able to reverse p300/CBP mediated acetylation of GR. In contrast to Suzuki et al. who reported that SIRT1 catalytic activity was dispensable for modulating GR function, we found that SIRT1, in the presence of its cofactor NAD^+, deacetylates GR *in vitro* (Figure 1E). Furthermore, overexpression of SIRT1 WT but not enzymatically inactive mutant (H363Y) reduced GR acetylation (Figure S1E). While SIRT1 and p300 have been implicated in GR-mediated transcription via regulating histone acetylation,[47] this is to our knowledge the first study reporting direct regulation of GR acetylation by these enzymes. HDAC2 was previously reported to deacetylate GR under inflammatory conditions.[19] Under Dex-treatment we rather observed a decrease in GR acetylation upon knockdown of HDAC2 and HDAC3 (Figures 1D and S1D) showing that they are not direct deacetylases of GR under these conditions.

Although acK154 correlated positively with GR transcriptional activity, mutation of Lys^{154} to Arg (acetylation-deficient) or Gln (acetylation-mimetic) did not abrogate GR-mediated target gene expression as seen by reporter assays and RNA-seq analysis after 6 h of Dex

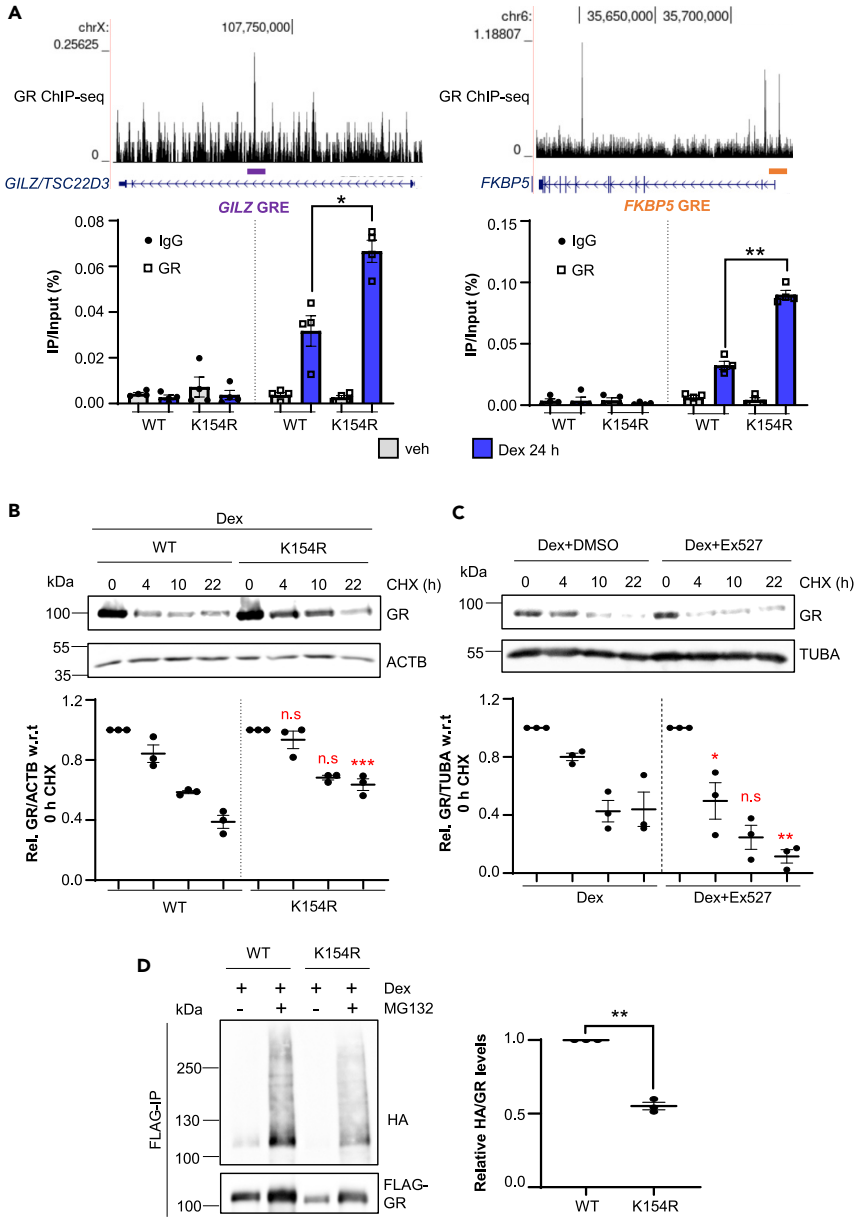

Figure 5. GR acetylation attenuates chromatin binding and protein stability upon prolonged GC exposure

(A) ChIP-qPCR showing *GILZ* (Gene name: *TSC22D3*) and *FKBP5* GRE occupancy of GR in HepG2 $GR^{-/-}$ + WT-GR and HepG2 $GR^{-/-}$ + K154R cells treated with vehicle or 1 μM Dex for 24 h. Scheme above shows qPCR amplicon positions for *GILZ* (purple) and *FKBP5* (orange) GRE with respect to GR ChIP-seq peaks in HepG2 cells from.[37] Data are shown as percentage of input. IgG served as a control for ChIP background.

(B) Western blot analysis of CHX chase experiment. HepG2 $GR^{-/-}$ cells transiently overexpressing Ty1-tagged WT or K154R-GR were treated with 1 μM Dex for 2 h followed by 20 ng/mL CHX for the indicated durations. Quantification shows GR/ACTB ratios normalized to respective 0 h CHX control.

(C) CHX chase experiment as in (B) performed in HepG2 cells treated with 1 μM Dex+DMSO or 1 μM Dex+20 μM Ex527. Quantification shows GR/TUBA ratios normalized to respective 0 h CHX controls.

(D) Western blot analysis of polyubiquitinated FLAG-GR immunoprecipitated from HEK239 $GR^{-/-}$ transiently expressing FLAG-tagged WT- or K154R-GR along with HA-UBB, treated with 1 μM Dex with or without 1 μM MG132 for 24 h. Quantification represents ratio of HA-UBB/GR signals from lanes 2 and 4 normalized to WT-Dex+MG132 (lane 2) sample. Data represent mean of n = 3 except for (A) where n = 4 independent experiments. Error bars = S.E.M. *p < 0.05, **p < 0.01, ***p < 0.001, n.s = non-significant; (B, C): One way ANOVA-Fischer's LSD test; (A) Student's paired t-test and (D) Welch's t-test.

See also Figure S5A.

exposure, indicating an ancillary role of this modification. RNA-seq data showed WT- and mutant- GR exert similar effects on Dex regulated genes at 6 h of Dex treatment. It has been suggested that hormone-dependent modifications may govern not only target gene specificity and cofactor recruitment, but also strength and duration of receptor activity.[46] Monitoring acK154 dynamics and GR-dependent

transactivation at different time points of Dex exposure revealed the temporal nature of acetylation-mediated regulation of GR function. Chromatin immunoprecipitation and subcellular fractionation experiments demonstrated that the GR-K154R mutant showed higher chromatin retention at longer Dex treatment time-points as compared to the wild-type (Figures 5A and S5A). RNA-seq analysis upon 24 h of Dex treatment would allow deciphering the changes in WT- and mutant-driven gene expression more robustly as the on-off kinetics of transcription are dependent on the gene context. Protein stability analysis showcased that the acetylation-deficient mutant of GR was degraded slower than the wild-type. Conversely, hyperacetylated GR in cells treated with Dex and the SIRT1 inhibitor Ex527, showed reduced stability and accelerated degradation (Figure 5). As the ubiquitin/proteasome system has been implicated in removal of GR from target DNA sites,[22,48] we show that acK154-GR is polyubiquitinated to a higher level than the K154R mutant, allowing its siphoning by the proteasome. We propose a model where acK154 correlates with GR activity but also seeds GR for degradation. This mode of transcription factor regulation has been observed for SREBP family and other transcription factors that undergo activity-coupled destruction to tune duration of the transcriptional response.[49,50] Acetylation-dependent polyubiquitination at Lys^{419} (human) within the PEST motif at the interface of NTD and DBD of GR,[22] might 'license' transcription by linking activity to degradation,[51] providing an additional layer of regulation. As GR is targeted by several E3 ubiquitin ligases in a cell-type and stimulus-dependent manner,[52] we speculate that the K154R mutant might show differential binding to one or more of these proteins as compared to the wild-type. Thus GR-K154 acetylation serves as a molecular timekeeper tuning the duration of GR activation by GCs. Levels of acetyl coenzyme A and NAD^+, that serve as cofactors for the GR modifying enzymes, are tightly controlled by the metabolic state of the cell. Future studies will unravel the role of GR acetylation as a node in GC signaling and metabolic pathways. As GC-dependent homologous down-regulation of GR has been implicated in the development of GC resistance under pathophysiological conditions,[7,52] our findings posit that controlling GR acetylation by SIRT1 or p300/CBP modulators alters GC responsiveness of cells in a temporal manner.

Limitations of the study

Our work has identified Lys^{154} as the dominant acetylation site in GR, which is critical for GR stability and duration of target gene activation. Accordingly, introduction of the acetylation-deficient K154R mutant stabilizes GR levels and sustains transcription of target genes. In contrast, we failed to observe a gain-of-function phenotype of the widely used acetylation-mimetic K→Q mutation, presumably because GR-K154Q does not faithfully emulate a constitutively acetylated lysine. Therefore, alternative strategies such as native chemical ligation or introduction of acetyl-lysine analogs[53] may help to circumvent this caveat, but their application *in vivo*, in mammalian systems are limited. Such a gain-of-acetylation mutant would enable dissecting the causal relationship of this modification to GR function.

In our study, we observed GR-acK154, in primary human cells such as HUVECs as well as mouse organs, demonstrating that this acetylation is an integral part of the GC-GR pathway. However, to further examine the physiological role of this modification, mouse models would be informative. Future studies replacing wild-type GR with the K154R mutant in mice would substantiate how acetylation impacts GC response dynamics in relation to stress and circadian rhythm.

STAR★METHODS

Detailed methods are provided in the online version of this paper and include the following:

- KEY RESOURCES TABLE
- RESOURCE AVAILABILITY
  - Lead contact
  - Materials availability
  - Data and code availability
- EXPERIMENTAL MODEL AND STUDY PARTICIPANT DETAILS
  - Cell culture and treatments
  - Animal experiments and ethics compliance
- METHOD DETAILS
  - Generation of stable cell lines
  - Transfections
  - Detection of GR acetylation
  - Detection of GR polyubiquitination
  - *In vitro* deacetylation assay
  - Chromatin immunoprecipitation
  - RNA extraction and expression analysis
  - RNA sequencing: Library preparation and analysis
  - Mass spectrometry
  - Immunofluorescence
  - Sequential immunoprecipitation
  - Cellular and subnuclear fractionation
  - Histone preparation

- Cycloheximide chase assay
- QUANTIFICATION AND STATISTICAL ANALYSIS

SUPPLEMENTAL INFORMATION

Supplemental information can be found online at https://doi.org/10.1016/j.isci.2024.108943.

ACKNOWLEDGMENTS

The authors thank Maren Godmann and Giorgio Caratti for critical discussions and pilot experiments in mice, respectively. We thank Holger Bierhoff for critical reading of the manuscript and providing NIH3T3 cells. We thank the researchers who provided plasmids and peptides (key resources table). We thank Regine Heller for providing HUVECs. We acknowledge the proteomics and next generation sequencing core facilities of the Fritz Lipmann Institute (FLI) for Aging, and Marco Groth for help with preparation and sequencing of cDNA libraries. We thank the University of Ulm animal facility for their excellent support. Schemes were created with BioRender.com. The authors thank the following funding agencies: Carl Zeiss Stiftung-IMPULS consortium (T.H.), DFG 177710919 - RTG 1715 (T.H.), IP 2021-08: IMPULSEproject Friedrich Schiller University, Jena (A.I.B.), DFG Research Training group-RTG 1715 (D.W.) and DFG CRC 1506 Aging at Interfaces (Project C05, Project Number 450627322) (J.P.T.).

AUTHOR CONTRIBUTIONS

A.I.B., M.W., and T.H. conceptualized the project. M.W. performed and analyzed initial experiments. A.I.B. and S.M.P. performed experiments. A.I.B. analyzed and interpreted data. M.W. and K.H.G. performed and analyzed mass spectrometry experiments. D.W. generated GR knockout cell lines. S.V. performed animal experiments. M.B. analyzed the RNA-seq data. T.H. and J.P.T. provided funding and supervision. A.I.B wrote the first draft of the manuscript. All authors contributed to revising the manuscript.

DECLARATION OF INTERESTS

Authors declare that they have no competing interests.

Received: August 15, 2023
Revised: November 30, 2023
Accepted: January 15, 2024
Published: January 18, 2024

REFERENCES

1. Weikum, E.R., Knuesel, M.T., Ortlund, E.A., and Yamamoto, K.R. (2017). Glucocorticoid receptor control of transcription: precision and plasticity via allostery. Nat. Rev. Mol. Cell Biol. *18*, 159–174.
2. Dostert, A., and Heinzel, T. (2004). Negative glucocorticoid receptor response elements and their role in glucocorticoid action. Curr. Pharmaceut. Des. *10*, 2807–2816.
3. Novac, N., Baus, D., Dostert, A., and Heinzel, T. (2006). Competition between glucocorticoid receptor and NFkappaB for control of the human FasL promoter. Faseb. J. *20*, 1074–1081.
4. Timmermans, S., Souffriau, J., and Libert, C. (2019). A General Introduction to Glucocorticoid Biology. Front. Immunol. *10*, 1545.
5. Vandewalle, J., Timmermans, S., Paakinaho, V., Vancraeynest, L., Dewyse, L., Vanderhaeghen, T., Wallaeys, C., Van Wyngene, L., Van Looveren, K., Nuyttens, L., et al. (2021). Combined glucocorticoid resistance and hyperlactatemia contributes to lethal shock in sepsis. Cell Metabol. *33*, 1763–1776.e5.
6. Wilkinson, L., Verhoog, N.J.D., and Louw, A. (2018). Disease- and treatment-associated acquired glucocorticoid resistance. Endocr. Connect. *7*, R328–R349.
7. Dendoncker, K., and Libert, C. (2017). Glucocorticoid resistance as a major drive in sepsis pathology. Cytokine Growth Factor Rev. *35*, 85–96.
8. Caratti, G., Stifel, U., Caratti, B., Jamil, A.J.M., Chung, K.J., Kiehntopf, M., Gräler, M.H., Blüher, M., Rauch, A., and Tuckermann, J.P. (2023). Glucocorticoid activation of anti-inflammatory macrophages protects against insulin resistance. Nat. Commun. *14*, 2271.
9. Vandevyver, S., Dejager, L., and Libert, C. (2014). Comprehensive Overview of the Structure and Regulation of the Glucocorticoid Receptor. Endocr. Rev. *35*, 671–693.
10. Kumar, R., and Thompson, E.B. (2012). Folding of the glucocorticoid receptor N-terminal transactivation function: Dynamics and regulation. Mol. Cell. Endocrinol. *348*, 450–456.
11. Lavery, D.N., and McEwan, I.J. (2005). Structure and function of steroid receptor AF1 transactivation domains: induction of active conformations. Biochem. J. *391*, 449–464.
12. Almlöf, T., Wallberg Ae Fau - Gustafsson, J.A., Gustafsson Ja Fau - Wright, A.P., and Wright, A.P. (1998). Role of important hydrophobic amino acids in the interaction between the glucocorticoid receptor tau 1-core activation domain and target factors. Biochemistry *37*, 9586–9594.
13. Kumar, R., Volk, D.E., Li, J., Lee, J.C., Gorenstein, D.G., and Thompson, E.B. (2004). TATA box binding protein induces structure in the recombinant glucocorticoid receptor AF1 domain. Proc. Natl. Acad. Sci. USA *101*, 16425–16430.
14. Rogatsky, I., Wang, J.C., Derynck, M.K., Nonaka, D.F., Khodabakhsh, D.B., Haqq, C.M., Darimont, B.D., Garabedian, M.J., and Yamamoto, K.R. (2003). Target-specific utilization of transcriptional regulatory surfaces by the glucocorticoid receptor. Proc. Natl. Acad. Sci. USA *100*, 13845–13850.
15. Ismaili, N., and Garabedian, M.J. (2004). Modulation of glucocorticoid receptor function via phosphorylation. Ann. N. Y. Acad. Sci. *1024*, 86–101.
16. Paakinaho, V., Lempiäinen, J.K., Sigismondo, G., Niskanen, E.A., Malinen, M., Jääskeläinen, T., Varjosalo, M., Krijgsveld, J., and Palvimo, J.J. (2021). SUMOylation regulates the protein network and chromatin accessibility at glucocorticoid receptor-binding sites. Nucleic Acids Res. *49*, 1951–1971.
17. Fryer, C.J., and Archer, T.K. (1998). Chromatin remodelling by the glucocorticoid receptor requires the BRG1 complex. Nature *393*, 88–91.
18. Suzuki, S., Iben, J.R., Coon, S.L., and Kino, T. (2018). SIRT1 is a transcriptional enhancer of the glucocorticoid receptor acting independently to its deacetylase activity. Mol. Cell. Endocrinol. *461*, 178–187.
19. Ito, K., Yamamura, S., Essilfie-Quaye, S., Cosio, B., Ito, M., Barnes, P.J., and Adcock, I.M. (2006). Histone deacetylase 2-mediated

deacetylation of the glucocorticoid receptor enables NF-kappaB suppression. J. Exp. Med. *203*, 7–13.
20. Nader, N., Chrousos, G.P., and Kino, T. (2009). Circadian rhythm transcription factor CLOCK regulates the transcriptional activity of the glucocorticoid receptor by acetylating its hinge region lysine cluster: potential physiological implications. Faseb. J. *23*, 1572–1583.
21. Deroo, B.J., Rentsch, C., Sampath, S., Young, J., DeFranco, D.B., and Archer, T.K. (2002). Proteasomal inhibition enhances glucocorticoid receptor transactivation and alters its subnuclear trafficking. Mol. Cell Biol. *22*, 4113–4123.
22. Wallace, A.D., Cao, Y., Chandramouleeswaran, S., and Cidlowski, J.A. (2010). Lysine 419 targets human glucocorticoid receptor for proteasomal degradation. Steroids *75*, 1016–1023.
23. Kino, T., and Chrousos, G.P. (2011). Acetylation-mediated epigenetic regulation of glucocorticoid receptor activity: circadian rhythm-associated alterations of glucocorticoid actions in target tissues. Mol. Cell. Endocrinol. *336*, 23–30.
24. Daley-Yates, P.T. (2015). Inhaled corticosteroids: potency, dose equivalence and therapeutic index. Br. J. Clin. Pharmacol. *80*, 372–380.
25. Diederich, S., Eigendorff, E., Burkhardt, P., Quinkler, M., Bumke-Vogt, C., Rochel, M., Seidelmann, D., Esperling, P., Oelkers, W., and Bähr, V. (2002). 11beta-hydroxysteroid dehydrogenase types 1 and 2: an important pharmacokinetic determinant for the activity of synthetic mineralo- and glucocorticoids. J. Clin. Endocrinol. Metab. *87*, 5695–5701.
26. Lempiäinen, J.K., Niskanen, E.A., Vuoti, K.M., Lampinen, R.E., Göös, H., Varjosalo, M., and Palvimo, J.J. (2017). Agonist-specific Protein Interactomes of Glucocorticoid and Androgen Receptor as Revealed by Proximity Mapping. Mol. Cell. Proteomics *16*, 1462–1474.
27. Presman, D.M., Ganguly, S., Schiltz, R.L., Johnson, T.A., Karpova, T.S., and Hager, G.L. (2016). DNA binding triggers tetramerization of the glucocorticoid receptor in live cells. Proc. Natl. Acad. Sci. USA *113*, 8236–8241.
28. Paakinaho, V., Johnson, T.A., Presman, D.M., and Hager, G.L. (2019). Glucocorticoid receptor quaternary structure drives chromatin occupancy and transcriptional outcome. Genome Res. *29*, 1223–1234.
29. Præstholm, S.M., Correia, C.M., and Grøntved, L. (2020). Multifaceted Control of GR Signaling and Its Impact on Hepatic Transcriptional Networks and Metabolism. Front. Endocrinol. *11*, 572981.
30. Payvar, F., DeFranco, D., Firestone, G.L., Edgar, B., Wrange, O., Okret, S., Gustafsson, J.A., and Yamamoto, K.R. (1983). Sequence-specific binding of glucocorticoid receptor to MTV DNA at sites within and upstream of the transcribed region. Cell *35*, 381–392.
31. Keenan, A.B., Torre, D., Lachmann, A., Leong, A.K., Wojciechowicz, M.L., Utti, V., Jagodnik, K.M., Kropiwnicki, E., Wang, Z., and Ma'ayan, A. (2019). ChEA3: transcription factor enrichment analysis by orthogonal omics integration. Nucleic Acids Res. *47*, W212–W224.
32. de Guia, R.M., and Herzig, S. (2015). How Do Glucocorticoids Regulate Lipid Metabolism? Adv. Exp. Med. Biol. *872*, 127–144.
33. Prus, G., Hoegl, A., Weinert, B.T., and Choudhary, C. (2019). Analysis and Interpretation of Protein Post-Translational Modification Site Stoichiometry. Trends Biochem. Sci. *44*, 943–960.
34. Bellingham, D.L., Sar, M., and Cidlowski, J.A. (1992). Ligand-dependent down-regulation of stably transfected human glucocorticoid receptors is associated with the loss of functional glucocorticoid responsiveness. Mol. Endocrinol. *6*, 2090–2102.
35. Fujimoto, H., Higuchi, M., Koike, M., Ode, H., Pinak, M., Bunta, J.K., Nemoto, T., Sakudoh, T., Honda, N., Maekawa, H., et al. (2012). A possible overestimation of the effect of acetylation on lysine residues in KQ mutant analysis. J. Comput. Chem. *33*, 239–246.
36. Molinari, E., Gilman, M., and Natesan, S. (1999). Proteasome-mediated degradation of transcriptional activators correlates with activation domain potency *in vivo*. EMBO J. *18*, 6439–6447.
37. Nakamoto, M., Ishihara, K., Watanabe, T., Hirosue, A., Hino, S., Shinohara, M., Nakayama, H., and Nakao, M. (2017). The Glucocorticoid Receptor Regulates the ANGPTL4 Gene in a CTCF-Mediated Chromatin Context in Human Hepatic Cells. PLoS One *12*, e0169225.
38. Ashton, A.W., Dhanjal, H.K., Rossner, B., Mahmood, H., Patel, V.I., Nadim, M., Lota, M., Shahid, F., Li, Z., Joyce, D., et al. (2024). Acetylation of nuclear receptors in health and disease: an update. FEBS J. *291*, 217–236.
39. Zee, B.M., and Garcia, B.A. (2012). Discovery of lysine post-translational modifications through mass spectrometric detection. Essays Biochem. *52*, 147–163.
40. Garza, A.M.S., Khan, S.H., and Kumar, R. (2010). Site-specific phosphorylation induces functionally active conformation in the intrinsically disordered N-terminal activation function (AF1) domain of the glucocorticoid receptor. Mol. Cell Biol. *30*, 220–230.
41. Weinert, B.T., Narita, T., Satpathy, S., Srinivasan, B., Hansen, B.K., Schölz, C., Hamilton, W.B., Zucconi, B.E., Wang, W.W., Liu, W.R., et al. (2018). Time-Resolved Analysis Reveals Rapid Dynamics and Broad Scope of the CBP/p300 Acetylome. Cell *174*, 231–244.e12.
42. Karr, J.P., Ferrie, J.J., Tjian, R., and Darzacq, X. (2022). The transcription factor activity gradient (TAG) model: contemplating a contact-independent mechanism for enhancer-promoter communication. Genes Dev. *36*, 7–16.
43. Morinière, J., Rousseaux, S., Steuerwald, U., Soler-López, M., Curtet, S., Vitte, A.L., Govin, J., Gaucher, J., Sadoul, K., Hart, D.J., et al. (2009). Cooperative binding of two acetylation marks on a histone tail by a single bromodomain. Nature *461*, 664–668.
44. Portuguez, A.S., Grbesa, I., Tal, M., Deitch, R., Raz, D., Kliker, L., Weismann, R., Schwartz, M., Loza, O., Cohen, L., et al. (2022). Ep300 sequestration to functionally distinct glucocorticoid receptor binding loci underlie rapid gene activation and repression. Nucleic Acids Res. *50*, 6702–6714.
45. Schulz, M., Eggert, M., Baniahmad, A., Dostert, A., Heinzel, T., and Renkawitz, R. (2002). RU486-induced glucocorticoid receptor agonism is controlled by the receptor N terminus and by corepressor binding. J. Biol. Chem. *277*, 26238–26243.
46. Wang, Z., Frederick, J., and Garabedian, M.J. (2002). Deciphering the phosphorylation "code" of the glucocorticoid receptor *in vivo*. J. Biol. Chem. *277*, 26573–26580.
47. Amat, R., Solanes, G., Giralt, M., and Villarroya, F. (2007). SIRT1 is involved in glucocorticoid-mediated control of uncoupling protein-3 gene transcription. J. Biol. Chem. *282*, 34066–34076.
48. Stavreva, D.A., Müller, W.G., Hager, G.L., Smith, C.L., and McNally, J.G. (2004). Rapid glucocorticoid receptor exchange at a promoter is coupled to transcription and regulated by chaperones and proteasomes. Mol. Cell Biol. *24*, 2682–2697.
49. Sundqvist, A., and Ericsson, J. (2003). Transcription-dependent degradation controls the stability of the SREBP family of transcription factors. Proc. Natl. Acad. Sci. USA *100*, 13833–13838.
50. Geng, F., Wenzel, S., and Tansey, W.P. (2012). Ubiquitin and proteasomes in transcription. Annu. Rev. Biochem. *81*, 177–201.
51. Salghetti, S.E., Caudy, A.A., Chenoweth, J.G., and Tansey, W.P. (2001). Regulation of transcriptional activation domain function by ubiquitin. Science *293*, 1651–1653.
52. Spies, L.L., Verhoog, N.J.D., and Louw, A. (2021). Acquired Glucocorticoid Resistance Due to Homologous Glucocorticoid Receptor Downregulation: A Modern Look at an Age-Old Problem. Cells *10*.
53. Kamieniarz, K., and Schneider, R. (2009). Tools to tackle protein acetylation. Chem. Biol. *16*, 1027–1029.
54. Spengler, K., Kryeziu, N., Grosse, S., Mosig, A.S., and Heller, R. (2020). VEGF Triggers Transient Induction of Autophagy in Endothelial Cells via AMPKalpha1. Cells *9*.
55. Graham, F.L., and van der Eb, A.J. (1973). A new technique for the assay of infectivity of human adenovirus 5 DNA. Virology *52*, 456–467.
56. Iyer-Bierhoff, A., Krogh, N., Tessarz, P., Ruppert, T., Nielsen, H., and Grummt, I. (2018). SIRT7-Dependent Deacetylation of Fibrillarin Controls Histone H2A Methylation and rRNA Synthesis during the Cell Cycle. Cell Rep. *25*, 2946–2954.e5.
57. Wieczorek, M., Gührs, K.H., and Heinzel, T. (2017). Assessment of HDACi-Induced Acetylation of Nonhistone Proteins by Mass Spectrometry. Methods Mol. Biol. *1510*, 313–327.
58. Bierhoff, H., Dammert, M.A., Brocks, D., Dambacher, S., Schotta, G., and Grummt, I. (2014). Quiescence-induced LncRNAs trigger H4K20 trimethylation and transcriptional silencing. Mol. Cell *54*, 675–682.
59. Bentley, D.R., Balasubramanian, S., Swerdlow, H.P., Smith, G.P., Milton, J., Brown, C.G., Hall, K.P., Evers, D.J., Barnes, C.L., Bignell, H.R., et al. (2008). Accurate whole human genome sequencing using reversible terminator chemistry. Nature *456*, 53–59.
60. Yan, Q., Wulfridge, P., Doherty, J., Fernandez-Luna, J.L., Real, P.J., Tang, H.Y., and Sarma, K. (2022). Proximity labeling identifies a repertoire of site-specific R-loop modulators. Nat. Commun. *13*, 53.

STAR★METHODS

KEY RESOURCES TABLE

REAGENT or RESOURCE	SOURCE	IDENTIFIER
Antibodies		
Pan acetyl-lysine	Cell Signaling Technology	Cat#9441; RRID:AB_331805
GCN5 (H-75)	Santa Cruz Biotechnology	Cat#sc-20698; RRID:AB_2128295
GR (H-300)	Santa Cruz Biotechnology	Cat#sc-8992; RRID:AB_2155784
GR (D6H2L) XP®	Cell Signaling Technology	Cat#12041; RRID:AB_2631286
His6 probe (H-3)	Santa Cruz Biotechnology	Cat#sc-8036; RRID:AB_627727
p300 (C-20)	Santa Cruz Biotechnology	Cat#sc-585; RRID:AB_2231120
CBP (A-22)	Santa Cruz Biotechnology	Cat#sc-369; RRID:AB_631006
PCAF (H-369)	Santa Cruz Biotechnology	Cat#sc-8999; RRID:AB_2128416
HDAC1 (10E2)	Santa Cruz Biotechnology	Cat# sc-81598; RRID:AB_2118083
HDAC2 (H-54)	Santa Cruz Biotechnology	Cat#sc-7899 RRID:AB_2118563
HDAC3 (H-99)	Santa Cruz Biotechnology	Cat#sc-11417; RRID:AB_2118706
SIRT1 (H-300)	Santa Cruz Biotechnology	Cat#sc-15404; RRID:AB_2188346
Beta-Actin	Sigma-Aldrich	Cat#A2066; RRID:AB_476693
Tubulin	Sigma-Aldrich	Cat#T5168; RRID:AB_477579
Vinculin	Bio-Rad	Cat#MCA465GA
HA-tag	Roche	Cat#1867423001; RRID:AB_390919
Ty1-tag	Diagenode	Cat#C15200054
FLAG-M2	Sigma-Aldrich	Cat#F3165; RRID:AB_259529
Anti-acetyl GR-K154	This study; Generated by Pineda antibodies	
Goat anti-rabbit-HRP conjugate	Jackson ImmunoResearch Labs	Cat#111-035-144; RRID:AB_2307391
Goat anti-mouse-HRP conjugate	Jackson ImmunoResearch Labs	Cat#115-035-062; RRID:AB_2338504
Normal rabbit IgG	Cell Signaling Technology	Cat#2729; RRID:AB_1031062
Normal mouse IgG	Sigma-Aldrich	Cat#12-371; RRID:AB_145840
Goat anti-Rabbit Alexa Fluor 594	Thermo Fischer Scientific	Cat#A-11012; RRID:AB_2534079
Chemicals, peptides, and recombinant proteins		
Dexamethasone (used for cell culture experiments)	Sigma-Aldrich	Cat#D4902
Dexamethasone (used for animal experiments)	Sigma-Aldrich	Cat#D2915
Prednisolone	Sigma-Aldrich	Cat#P6004
Hydrocortisone	Sigma-Aldrich	Cat#H2270
Mifepristone (RU486)	Sigma-Aldrich	Cat#M8046
A485	Tocris	Cat#6387
Ex527 (Selisistat)	Selleckchem	Cat#S1541
Nicotinamide	Sigma-Aldrich	Cat#N0636
Trichostatin A	Sigma-Aldrich	Cat#T8552
Nicotinamide Adenine Dinucleotide sodium salt	Sigma-Aldrich	Cat#N1636
Flavopiridol	Sigma-Aldrich	Cat#F3055
Cycloheximide	Sigma-Aldrich	Cat#C4859
Doxycycline	Clontech	Cat#631311
Puromycin	Sigma-Aldrich	Cat#P8833

(*Continued on next page*)

Continued

REAGENT or RESOURCE	SOURCE	IDENTIFIER
MG132	Merck/Sigma-Aldrich	Cat#C2211
Recombinant human SIRT1	Enzo Life Sciences	Cat#BML-SE239-0100
3X FLAG peptide	Sigma-Aldrich	Cat#F4799
Acetylated K154 peptide: H-CAPTEK(ac)EFPK-NH_2	This study; Synthesized by D. Imhof, University of Bonn	
Non-acetylated K154 peptide: H-CAPTEKEFPK-NH_2	This study; Synthesized by D. Imhof, University of Bonn	
Critical commercial assays		
Dual Luciferase Assay	Promega	Cat#E1910
NEBNext Ultra II Directional RNA Library Preparation Kit	New England Biolabs	Cat#E7760
NEBNext Poly(A) mRNA Magnetic Isolation Module	New England Biolabs	Cat#E7490
NEBNext Multiplex Oligos for Illumina (Unique Dual Index UMI Adaptors RNA Set 1)	New England Biolabs	Cat#E7416
Deposited data		
RNA-sequencing data	This study	GEO database: GSE236739
Experimental models: Cell lines		
HepG2	DSMZ	Cat#ACC 180
HepG2 $GR^{-/-}$	This study	
HepG2 $GR^{-/-}$+Ty1-WT-GR	This study	
HepG2 $GR^{-/-}$+Ty1-K154R-GR	This study	
HepG2 $GR^{-/-}$+Ty1-K154Q-GR	This study	
HEK293	DSMZ	Cat#ACC 305
HEK293 $GR^{-/-}$	This study	
HeLa	DSMZ	Cat#ACC 57
BHK-21	DSMZ	Cat#ACC 61
A549	Tuckermann lab, University of Ulm	
NIH3T3	Gift from H.Bierhoff, Friedrich Schiller University, Jena	
HEK293T	Gift from I. Grummt, German Cancer Research Centre	
HUVEC	Gift from R.Heller, University Hospital, Jena	
Experimental models: Organisms/strains		
C57BL/6 wild-type mice	Tuckermann lab, University of Ulm	
Oligonucleotides		
siRNAs, shRNAs and sgRNAs used in this study	See Table S1	
Primers used in this study	See Table S4	
Recombinant DNA		
pRK7-FLAG-GR	Gift from T. Rein (Max Planck Institute for Psychiatry, Munich)	
CBP-FLAG	Gift from R. Eckner (University of New Jersey)	
pCMV-p300-HA	Gift from R. Eckner (University of New Jersey)	
pCX-FLAG-PCAF	Gift from T. Kouzarides (University of Cambridge)	

(*Continued on next page*)

Continued

REAGENT or RESOURCE	SOURCE	IDENTIFIER
pACT2-His6-TIP60	Gift from K. Coffey (Newcastle University)	
pHH-MMTV-luc	Gift from S. Nordeen (University of Colorado)	
pBABE-SIRT1	Gift from R. Weinberg (University of Connecticut School of Medicine)	
pEGFP-C3-mGR WT and mono (A465T/I634A), tetra (P481R) mutants	Gift from G. Hager (National Institute for Health)	
pX330-U6-Chimeric_BB-CBh-hSpCas9-GFP	Gift from J. Müller (University Hospital, Jena)	
pEGFP-C1-SIRT1	Gift from I. Grummt (German Cancer Research Centre)	
pEGFP-C1-SIRT7	Gift from I. Grummt (German Cancer Research Centre)	
pCW57-MCS1-2A-MCS2	Addgene	Cat#71782
pCW57-MCS1-2A-MCS2-Ty1-WT-GR	This study	
pCW57-MCS1-2A-MCS2-Ty1-K154R-GR	This study	
pCW57-MCS1-2A-MCS2-Ty1-K154Q-GR	This study	
pLenti6-UBC-mSLC7A1	Addgene	Cat#17224
pHCMV-EcoEnv	Addgene	Cat#15802
pMDLg/pRRE	Addgene	Cat#12251
pRSV-Rev	Addgene	Cat#12253
pcDNA3.1-HA-UBB	This study; Custom synthesized by Biocat	
pcDNA3.1-Ty1-WT-GR	This study; Custom synthesized by Biocat	
pcDNA3.1-Ty1-K154R-GR	This study; Custom synthesized by Biocat	
pcDNA3.1-Ty1-K154Q-GR	This study; Custom synthesized by Biocat	
Software and algorithms		
ProteomeDiscoverer v1.4	Thermo Fischer Scientific	
Mascot v2.4	Matrix Science	
bcl2fastq v2.20.0.422	Illumina	RRID:SCR_015058
FASTQC v0.11.9		RRID:SCR_014583
cutadapt v3.7		RRID:SCR_011841
STAR v2.7.6a		RRID:SCR_004463
featureCounts v2.0.3		RRID:SCR_012919
DESeq2		RRID:SCR_015687
limma v3.50.3		RRID:SCR_010943
clusterProfiler v4.2.2		RRID:SCR_016884
ImageJ		RRID:SCR_003070
GraphPad Prism		RRID:SCR_002798

RESOURCE AVAILABILITY

Lead contact

Further information and requests for resources and reagents should be directed to and will be fulfilled by the lead contact, Thorsten Heinzel (t.heinzel@uni-jena.de).

Materials availability

Plasmids, cell lines and antibodies generated in this study are available upon request to the lead contact, under a Materials Transfer Agreement with the Friedrich Schiller University of Jena.

Data and code availability

- RNA-seq data have been deposited at the Gene Expression Omnibus (GEO) database and are publicly available as of the date of publication. Accession number is listed in the key resources table.
- The paper does not report original code.
- Any additional information required to reanalyze the data reported in this paper is available from the lead contact upon request.

EXPERIMENTAL MODEL AND STUDY PARTICIPANT DETAILS

Cell culture and treatments

Baby hamster kidney (BHK-21), mouse embryonic fibroblast (NIH3T3), human embryonic kidney (HEK293) and human lung adenocarcinoma A549 cells and their derivative cell lines were cultured in DMEM (Sigma) supplemented with 10% fetal calf serum (FCS) (Capricorn) and 1000 U penicillin/100 μg/mL streptomycin (1% Pen-strep) solution (Sigma). Human cervical cancer-derived HeLa cells, hepatocarcinoma HepG2 and its derivative cell lines were maintained in RPMI1640/10% FCS/1% Pen-strep medium. HepG2 cells were used at passage numbers < 15 to ensure high responsiveness to GCs with respect to both gene expression and acK154 levels. Human umbilical vein endothelial cells (HUVEC) were isolated by the Heller lab, from anonymously acquired umbilical cords after obtaining informed consent from donors, according to the Declaration of Helsinki, "Ethical principles for Medical Research Involving Human Subjects" (1964).[54] Jena University Hospital Ethics Committee approved the study (no. 2023-2894). HUVECs were cultured in Medium 199 (Lonza) containing 17.5% FBS, 2.5% autologous serum, 1% Pen-Strep solution, 680 μM L-Glutamine, 24.8 μg/ml heparin, 0.25% ECGS and 80 μM ascorbic acid. All cells were maintained under standard aseptic conditions at 5% CO_2 and 37°C. Cells were cultured for at least 24 hours in charcoal-stripped serum containing medium prior to glucocorticoid treatment. Cells were treated with 1 μM of the relevant glucocorticoid (Dex or RU486 or prednisolone or hydrocortisone-Sigma-Aldrich) (unless otherwise mentioned) for the time points indicated in the respective figure legends. Ex527 (Selisistat-Selleckchem) and A485 (Tocris Bioscience) were used to inhibit SIRT1 and p300/CBP at concentrations of 20 μM and 5 μM respectively for durations as indicated.

Animal experiments and ethics compliance

Wild-type mice (C57BL/6) (12-18 weeks, males and females) were bred in the animal facility at the University of Ulm and were housed single-caged one week prior to the experiment. The animals were treated in the morning with vehicle (PBS) or 1 mg/kg Dex i.p. (Sigma-Aldrich, #D2915, reconstituted in PBS) and were killed 6 hours later by decapitation to minimize stress levels and thereby prevent a spike in the endogenous corticosterone levels. Organs were harvested and snap frozen in liquid nitrogen until further use. Organ lysates were prepared and analyzed for GR K154 acetylation by western blotting as described in the section 'Detection of GR acetylation'. Western blot shows representative image from two mice per group. This study was approved by the federal authorities for animal research of the Regierungspräsidium Tübingen, Baden-Wuerttemberg, Germany and performed in adherence with the National Institutes of Health Guidelines on the Use of Laboratory Animals, and the European Union 'Directive 2010/63 EU on the protection of animals used for scientific purposes'.

METHOD DETAILS

Generation of stable cell lines

To generate GR knockout cells HEK293 and HepG2 cells were transfected with a pool of three different pX330-U6-Chimeric_BB-CBh-hSpCas9-GFP (kind gift from J. Müller) constructs harboring the annealed oligonucleotides encoding three distinct single guide (sg) RNAs (Table S3), using Lipofectamine 3000 reagent (Thermo Fischer Scientific) according to manufacturer's protocol. Cells transfected with the empty vector alone served as control. 48 hours post-transfection, GFP positive/DAPI negative cells were sorted into 96 well plates containing conditioned media. Cells were expanded and genomic indels in the *NR3C1* gene were monitored by PCR and sequencing. Loss of GR protein was confirmed by western blotting. HepG2 $GR^{-/-}$ cells were transfected with pLenti6-UBC-mSLC7A1 (Addgene #17224) to transiently express ecotropic receptor protein mSLC7A1 (mCAT1) and transduced with pseudotyped lentiviral pCW57-MCS1-2A-MCS2 vector (Addgene #71782) harboring Ty1-tagged human *NR3C1* wildtype or mutant cDNA. Infected cells were selected for 2 weeks with 2 μg/mL puromycin (Sigma-Aldrich) and characterized for doxycycline (0.3 -1 μg/mL) inducible expression of GR by western blotting. To ensure equal expression of Ty1-WT, K154R and K154Q-GR and comparable expression to endogenous GR in HepG2 $GR^{+/+}$ cells, adjusted doxycycline doses were used to induce GR expression for 24 hours followed by a washout step and addition of fresh charcoal-stripped FCS containing media devoid of doxycycline for another 24 h where also the Dex treatments (6 or 24 hours) were performed.

Transfections

Cells were seeded in culture media and allowed to attach for 24 hours. Cells were transfected with 40 nM siRNAs (see Table S3) using Lipofectamine 3000 reagent (Thermo Fischer Scientific) in FCS-free OptiMEM. Medium was exchanged 18 hours post-transfection and cells were harvested after about 30 hours. DNA transfections were performed using Lipofectamine 2000 or 3000 (HepG2, HeLa and BHK-21) according to manufacturer's protocol or using the calcium phosphate method (HEK293 or HEK293T) as these cell lines served to be suitable hosts for transfections and manipulation.[55]

Detection of GR acetylation

Detection of acetylation was performed as in.[56,57] Briefly, for global acetylation of GR, cells expressing FLAG- or Ty1- tagged GR were lysed in radioimmunoprecipitation assay (RIPA) buffer (50 mM Tris-HCl [pH 8.0], 150 mM NaCl, 1 mM EDTA [pH 8.0], 1 mM EGTA [pH 8.0], 1% NP-40, 1% sodium deoxycholate, 0.1% SDS) supplemented with protease inhibitors (100 mM PMSF, aprotinin, leupeptin), phosphatase inhibitors (10 mM sodium orthovanadate, 0.5 mM sodium fluoride) and lysine deacetylase inhibitors including 1 μM trichostatin A (TSA) and 10 mM nicotinamide (NAM). Cell suspensions were sonicated with a Branson sonifier and cleared by high-speed centrifugation. Anti-FLAG M2 agarose beads (Sigma-Aldrich) or Protein A/G sepharose beads coupled to 5 μg anti-Ty1 antibody, were incubated with lysates overnight at 4°C with constant rotation. Following three washes with lysis buffer, the immunoprecipitates were eluted in 2X Laemmli buffer for analysis of GR acetylation using pan acetyl-lysine antibody in western blotting. GR-acK154 was detected in whole cell extracts or nuclear extracts in RIPA buffer as stated above, using self-generated site-specific antibodies (Pineda).

Detection of GR polyubiquitination

HEK293 $GR^{-/-}$ cells were transfected with FLAG-tagged WT- or K154R-GR (pRK7-FLAG-GR) in combination with HA-tagged UBB (pcDNA3.1 HA-UBB; HA-UBB cDNA sequence [GenBank: NM_018955.4] with N-terminal HA-tag cloned into HindIII/EcoRI of pcDNA3.1) each, using the calcium phosphate method.[55] Cells were treated with 1 μM Dex alone or in combination with 1 μM MG132 (Sigma-Aldrich) for 24 h followed by harvesting, cell lysis and FLAG-IP as stated in the above section. Lysis/wash buffer was supplemented with 10 mM N-ethylmaleimide (NEM) in addition to other inhibitors to preserve the ubiquitination of proteins upon cell lysis. Immunoprecipitates were eluted by boiling beads in 2X Laemmli buffer, followed by SDS-PAGE and western blotting with anti-HA (Roche) and anti-GR (Cell Signaling Technology) antibodies.

In vitro deacetylation assay

BHK-21 cells transiently overexpressing FLAG-GR were treated with 1 μM Dex and 20 μM Ex527 for 16 hours. Cells were lysed and anti-FLAG immunoprecipitation was performed as stated above. Bead coupled GR-FLAG was washed five times with 50 mM Tris-HCl [pH 8.0], 137 mM NaCl, 2.7 mM KCl, 1 mM $MgCl_2$ and 1 mg/ml BSA. Beads were incubated in the same buffer containing 1 or 3 U recombinant human SIRT1 (Enzo Life Sciences) in the presence or absence of 0.5 mM NAD^+ (Sigma-Aldrich) with or without 20 μM Ex-527 at 37°C for 30 min. Reaction was stopped by addition of 2X Laemmli buffer, heating at 95°C for 10 minutes followed by SDS-PAGE and western blotting.

Chromatin immunoprecipitation

ChIP assays were performed according to.[58] Briefly, HepG2 $GR^{-/-}$ + Ty1-GR cells were crosslinked with 1% formaldehyde for 10 minutes at room temperature followed by quenching with 125 mM glycine for 5 minutes. Cells were washed and harvested in cold PBS. Cells were consecutively incubated in buffer A (100 mM Tris-HCl [pH 8], 10 mM DTT) for 15 min on ice, 15 min at 30°C followed by buffer B (10 mM HEPES [pH 7.5], 10 mM EDTA, 0.5 mM EGTA, 0.25% Triton X-100) for 5 min on ice, followed by buffer C (10 mM HEPES [pH 7.5], 10 mM EDTA, 0.5 mM EGTA, 200 mM NaCl) for 5 min on ice. Nuclei were lysed in buffer D (50 mM Tris-HCl [pH 8], 10 mM EDTA, 1% SDS) and chromatin was sheared in a Bioruptor (Diagenode) to achieve fragment sizes 150-500 bp. Sonicated chromatin was cleared and diluted 5 times with ChIP dilution buffer (15 mM Tris-HCl [pH 8], 180 mM NaCl, 1.2 mM EDTA, 1.2% Triton X-100). 15-20 μg chromatin was incubated overnight at 4°C with antibodies coupled to protein G dynabeads (Invitrogen) blocked with BSA and herring sperm DNA: for GR ChIP a cocktail of 5 μl anti-GR D6H2L-XP rabbit monoclonal (Cell signaling Technology), 1 μg anti-GR H-300 rabbit polyclonal (Santa Cruz) and 5 μg of Ty1 (Diagenode) monoclonal antibodies was used and mouse/rabbit IgG (Sigma-Aldrich/Cell Signaling Technology) served as control. Beads were successively washed in low salt buffer (20 mM Tris-HCl [pH 8.0], 150 mM NaCl, 2 mM EDTA, 0.1% SDS, 1% Triton X-100), high salt buffer (20 mM Tris-HCl [pH 8.0], 500 mM NaCl, 2 mM EDTA, 0.1% SDS, 1% Triton X-100), LiCl buffer (10 mM Tris-HCl [pH 8.0], 250 mM LiCl, 1 mM EDTA, 1% sodium deoxycholate, 1% NP-40) and TE buffer (10 mM Tris-HCl [pH 8], 1 mM EDTA). Bound DNA was eluted in 100 mM sodium bicarbonate, 1% SDS-containing buffer, followed by decrosslinking overnight at 65°C in the presence of 300 mM NaCl and 10 μg DNAse-free RNAse. IP and input DNA were purified with ChIP DNA clean and concentrator columns (Zymo) and used subsequently for SYBR green chemistry (Thermo Fischer Scientific)-based qPCR using primers listed in Table S4.

RNA extraction and expression analysis

Cells were harvested in TRIzol (Ambion) and mixed with bromochloropropane (BCP) (10% volume of TRIzol lysate). Samples were vortexed, centrifuged at 18,000 g for 15 min at 4°C. Aqueous phase was mixed with equal volume of isopropanol and 20 μg glycogen (Thermo Fischer Scientific) followed by incubation on ice for 30 minutes. RNA was precipitated by high- speed centrifugation as above and the pellet was washed twice in 70% ethanol followed by air drying. RNA was reconstituted by resuspension in nuclease-free water and agitation at 56°C for 15 minutes. Nanodrop was used to measure RNA concentration and quality. To remove any phenol or protein contamination, RNA was re-precipitated overnight at -20°C or 1 hour at -80°C in three volumes of absolute ethanol and $1/10^{th}$ volume of 3 M sodium acetate pH 5, followed by washes in 70% ethanol and reconstitution in nuclease-free water. RNA was processed either into libraries for Illumina sequencing or cDNA as follows. To remove genomic DNA contaminants, RNA was treated with RNAse-free DNAse (Thermo Fischer Scientific) followed by reverse transcription using a mix of oligo (dT) and random hexamers according to the manufacturer's protocol (Thermo Fischer Scientific). RT-qPCR was performed using SYBR green (Thermo Fischer Scientific) chemistry with primers listed in Table S4.

RNA sequencing: Library preparation and analysis

Sequencing of RNA samples was performed using Illumina's next-generation sequencing methodology.[59] Briefly, total RNA was quantified and quality checked using Agilent 4200 TapeStation Instrument in combination with RNA ScreenTape. Libraries were prepared from 300 ng of input material using NEBNext Ultra II Directional RNA Library Preparation Kit in combination with NEBNext Poly(A) mRNA Magnetic Isolation Module and NEBNext Multiplex Oligos for Illumina (Unique Dual Index UMI Adaptors RNA Set 1) following the manufacturer's instructions (New England Biolabs). Quantification and quality check of libraries was performed using Agilent 4200 Tapestation Instrument in combination with D5000 ScreenTape. Libraries were pooled and sequenced on NovaSeq6000 using SP Reagent Kit v1.5 (100 cycles) and 101 single-end workflows. Total and uniquely mapped read counts for each sample are provided in Table S5. Sequence information was converted to FASTQ format using bcl2fastq v2.20.0.422. Raw FASTQ data underwent quality control using FASTQC (version 0.11.9). Quality trimming, adapter and poly(A) clipping were performed using cutadapt (version 3.7; parameter: -q 10 -m 30 - -a AGATCGGAAGAGCACACGTCTG AACTCCAGTCA). Preprocessed reads were aligned to reference genome (GRCh38.p13) using STAR (version 2.7.6a; parameter: –outSAM-multNmax 1 –outSJfilterReads Unique –outFilterMultimapNmax 1 –outFilterMismatchNoverLmax 0.04 –alignIntronMax 1000000 –sjdbOverhang 99). Gene expression was quantified using featureCounts (version 2.0.3) and Ensembl Release 100 gene annotation. Downstream analyses were conducted in R programming environment (version 4.1.3). Principle component analysis of normalized gene counts (variance stabilizing transformation) revealed that date of RNA isolation was a confounding factor. Therefore, modelling of this batch effect was included in design formula of DESeq2 (version: 1.34; model: ~batch + group) to determine genotype-specific differentially expressed genes between experimental groups while accounting for batch effects (FDR < 0.05 and baseMean > 5). Likelihood ratio test (DESeq2) was performed to compare the full model '~batch + background + treatment + genotype:treatment' to the reduced model '~batch + genotype + treatment'. This analysis specifically returns genes that show significant changes between genotypes due to effect of treatment. For visualization, batch effect was removed using 'removeBatchEffect' (limma, version 3.50.3) from variance stabilized counts (PCA shown in Figure S4F). Functional enrichment analysis was performed using clusterProfiler (version 4.2.2) focusing on commonly differentially expressed genes across genotypes.

Mass spectrometry

BHK-21 or HeLa cells were transfected with FLAG-GR and then treated with 1 μM Dex in combination with 10 mM NAM or 20 μM Ex527 for 16 hours. Following lysis and immunoprecipitation with M2-agarose beads as described in the aforementioned section, FLAG-GR immunoprecipitates were resolved by SDS-PAGE, stained with Coomassie G-250, the correct band was sliced out followed by destaining, alkylation of cysteines and tryptic digest. Peptides were subjected to nano-liquid electrospray ionized tandem mass spectrometry (LC-ESI-MS/MS) using an LQ Orbitrap XL ETD (Thermo Fischer Scientific) as described in.[57] The mass spectrometer was set up to scan the full spectrum ranging from 300 to 2000 Da followed by three MS/MS spectra after CID (collision induced dissociation) fragmentation of multiple charged precursors. Peptide sequences were attributed to the spectra using ProteomeDiscoverer software (v1.4, Thermo Fischer Scientific) in combination with Mascot (v2.4 Matrix Science) and the Swiss-Prot database (www.uniprot.org). Lysine sites that were identified to be acetylated with high confidence in at least one experiment have been annotated.

Immunofluorescence

Cells were fixed in 4 % formaldehyde/PBS for 10 minutes at room temperature followed by permeabilization with ice cold 0.5% Triton X-100/PBS for 15 minutes on ice. Blocking was performed in 3 % BSA/PBS-0.05% Tween-20 for 1 hour at room temperature. Coverslips were incubated overnight at 4°C with anti-GR (Cell signaling #12041) antibody diluted in blocking buffer, in a humidified chamber. Coverslips were washed in PBS and incubated for 1 hour at room temperature with Alexa Fluor 594 anti-rabbit secondary antibody (Invitrogen) and Alexa Fluor 488-conjugated phalloidin stain (Invitrogen) in 0.3% BSA/PBS-0.05% Tween-20. Cells were washed and counterstained with 1 μg/mL Hoechst 33342 in PBS for 10 minutes followed by PBS washes and mounting with Fluoromount-G solution (Invitrogen). Samples were analyzed with a Nikon epifluorescence microscope.

Sequential immunoprecipitation

Cells were lysed in NT buffer (300 mM NaCl, 50 mM Tris-HCl [pH 8.0], 1% Triton X-100, 0.1% NP-40, 1 mM EDTA [pH 8.0], 1 mM EGTA [pH 8.0])-containing protease, phosphatase and deacetylase inhibitors and immunoprecipitation with anti-FLAG M2 beads or mouse IgG- bound protein A/G beads was performed for 3 hours at 4°C with constant rotation. After three washes in lysis buffer, immunoprecipitates were eluted twice in FLAG peptide elution buffer (NT lysis buffer+ 800 ng/μL FLAG-peptide) for 2 hours each at 4°C with constant rotation, and were saved as eluate1 M2 and eluate1 IgG respectively. These eluates served as input2 for a second IP with site-specific anti-acK154 antibodies that were then captured with protein A/G sepharose beads. Beads were washed three times in lysis buffer followed by elution in 2X Laemmli buffer. Inputs, flow-through (supernatant after IP) and eluates were analyzed by SDS-PAGE and western blotting.

Cellular and subnuclear fractionation

To obtain cytoplasmic and nuclear fractions, cells were resuspended in hypotonic buffer (10 mM HEPES [pH 7.9], 10 mM KCl, 1.5 mM $MgCl_2$, 0.34 M sucrose, 10% (v/v) glycerol and 1 mM DTT) supplemented with protease, phosphatase and HDAC inhibitors, followed by addition of 0.1% (v/v) Triton X-100 and incubation on ice for 8 minutes. Lysis of the cell membrane and release of nuclei was confirmed by brightfield

microscopy, and nuclei (pellet) were separated from the cytoplasmic fraction (supernatant) by centrifugation at 1300 g for 10 minutes at 4°C. Nuclear pellets were washed once in hypotonic buffer without Triton X-100 followed by resuspension in buffer S1 (0.25 M Sucrose, 10 mM $MgCl_2$). Nuclear suspension was layered over equal volume of buffer S2 (0.35 M Sucrose, 0.5 mM $MgCl_2$) and centrifuged at 1300 g for 5 minutes, 4°C. Nuclear pellets were lysed in RIPA lysis buffer and processed as described earlier for whole cell lysates.

Subnuclear fractionation was performed as described in.[60] Briefly, cells were resuspended in Buffer A (10 mM HEPES [pH 7.5], 5 mM $MgCl_2$, 0.25 M sucrose, 0.1% NP-40) and incubated on ice for 10 min followed by centrifugation at 6000 g at 4°C for 10 min. The supernatant (cytoplasmic fraction) was discarded, and nuclear pellet was resuspended in Buffer B (10 mM HEPES [pH 7.5], 0.1 mM EDTA, 1.5 mM $MgCl_2$, and 25% glycerol). About 30% of the suspension was supplemented with 2.5 M KCl to a final concentration of 500 mM KCl, sonicated with a Branson sonifier and cleared by high-speed centrifugation. The supernatant served as total nuclear extract. The remaining 70% of the nuclear pellet suspension in Buffer B was adjusted to 300 mM KCl by addition of 2.5 M KCl and incubated on ice for 15 min. The nuclei were centrifuged at 9400 g at 4°C for 15 min and supernatant was transferred to new tubes as the nuclear-soluble fraction. The remaining pellet was resuspended in Buffer B containing 1 M KCl and lysed on ice for 20 min. Salt concentration was reduced to 350 mM by addition of Buffer B followed by sonication, centrifugation at 9400 g at 4°C for 15 min. 10% of each fraction was used for western blot.

Histone preparation

Cells were harvested followed by lysis in PBS/0.5% Triton X-100, and isolated nuclei were incubated in 0.2 N HCl at 4°C overnight with rotation. Extracts were cleared by centrifugation and pH was neutralized with 0.1 volume of 1 M Tris base (Sigma-Aldrich). For western blotting, 2 μg of histones were loaded on 15% SDS polyacrylamide gels.

Cycloheximide chase assay

Cells expressing WT or K154R-GR or wild-type cells expressing endogenous GR were respectively treated with 1 μM Dex or Dex (1 μM) +Ex527 (20 μM) for 2 hours followed by treatment with 20 ng/mL cycloheximide (CHX) (Sigma-Aldrich #C4859) for 4, 10 and 22 hours. Cells were harvested after 2 hours of Dex or Dex+Ex527 treatment (0 h CHX control) or at the indicated times after Dex+CHX (or Dex+Ex527+CHX) treatment and subjected to lysis followed by SDS-PAGE and western blotting.

QUANTIFICATION AND STATISTICAL ANALYSIS

All data are representative of at least three or four biological replicates as indicated in the figure legends. Experiments involving HepG2 $GR^{-/-}$ +Ty1-WT or mutant GR were performed with cell lines obtained after two independent transductions, and two biological replicates from each of the transductions such that n=4. Quantification of western blot signals was performed by densitometric analyses using ImageJ.

Statistical significance was calculated with Welch's t-test or Welch's ANOVA test with Dunnett's T3 correction when comparing western blot quantification from two or more groups respectively. As western blot signals are set to one for the controls, samples represent values with unequal variance. In Figure 5 one-way ANOVA with Fischer's LSD test was used to compare between western blot signals as the normalization was performed to the control sample but the comparisons were between the (2+4h) samples of WT and K154R and so on for the other two time points. One-way ANOVA with Fischer's LSD test was used for RT-qPCR data (log2 fold change) when comparing only three groups using GraphPad Prism. Significance level was set to $\alpha = 0.05$ and *$p < 0.05$, **$p < 0.01$, ***$p < 0.001$, ****$p < 0.0001$ and n.s = non-significant.